

New Jersey Institute of Technology Digital Commons @ NJIT

Theses

Theses and Dissertations


Fall 2017

Computational and experimental determination of the mixing efficiency of a microfluidic serpentine micromixer

Siril Arockiam

New Jersey Institute of Technology

Follow this and additional works at: <https://digitalcommons.njit.edu/theses>

 Part of the [Biochemical and Biomolecular Engineering Commons](#), and the [Pharmaceutics and Drug Design Commons](#)

Recommended Citation

Arockiam, Siril, "Computational and experimental determination of the mixing efficiency of a microfluidic serpentine micromixer" (2017). *Theses*. 41.
<https://digitalcommons.njit.edu/theses/41>

This Thesis is brought to you for free and open access by the Theses and Dissertations at Digital Commons @ NJIT. It has been accepted for inclusion in Theses by an authorized administrator of Digital Commons @ NJIT. For more information, please contact digitalcommons@njit.edu.

Copyright Warning & Restrictions

The copyright law of the United States (Title 17, United States Code) governs the making of photocopies or other reproductions of copyrighted material.

Under certain conditions specified in the law, libraries and archives are authorized to furnish a photocopy or other reproduction. One of these specified conditions is that the photocopy or reproduction is not to be “used for any purpose other than private study, scholarship, or research.” If a user makes a request for, or later uses, a photocopy or reproduction for purposes in excess of “fair use” that user may be liable for copyright infringement,

This institution reserves the right to refuse to accept a copying order if, in its judgment, fulfillment of the order would involve violation of copyright law.

Please Note: The author retains the copyright while the New Jersey Institute of Technology reserves the right to distribute this thesis or dissertation

Printing note: If you do not wish to print this page, then select “Pages from: first page # to: last page #” on the print dialog screen

The Van Houten library has removed some of the personal information and all signatures from the approval page and biographical sketches of theses and dissertations in order to protect the identity of NJIT graduates and faculty.

ABSTRACT

COMPUTATIONAL AND EXPERIMENTAL DETERMINATION OF THE MIXING EFFICIENCY OF A MICROFLUIDIC SERPENTINE MICROMIXER

**by
Siril Arockiam**

In microfluidics, efficiency and mixing time are the greatest disadvantages. These parameters hinder the application of microfluidic devices for biochemical and immunological assays. However, once these disadvantages have been overcome by optimizing the parameters of the microfluidic device, it becomes an important analytical tool. In this experiment, various designs of microfluidic devices have been both simulated using COMSOL software, and experimentally verified to obtain the optimized parameter such as depth and velocity for better mixing efficiency. The COMSOL model has been validated by comparing the results with fluorescent images data of the experiment. The microfluidic device is built with adhesive double-sided tape and glass slides. The microfluidic channels are 25 μ m in depth and 700 μ m in width. These channels have a serpentine design with three loops. It was analyzed that by increasing the depth of the channel to 400 μ m at 0.1 μ l/min flow rate, 99.5% mixing efficiency was obtained. As both the contact area and time were increasing, which in turn lead to the increase in diffusion mixing between the two streams.

**COMPUTATIONAL AND EXPERIMENTAL DETERMINATION OF THE
MIXING EFFICIENCY OF A MICROFLUIDIC SERPENTINE
MICROMIXER**

**By
Siril Arockiam**

**A Thesis
Submitted to the Faculty of
New Jersey Institute of Technology
In Partial Fulfillment of the Requirements for the Degree of
Master of Science in Biopharmaceutical Engineering**

**Otto H. York Department of
Chemical, Biological and Pharmaceutical Engineering**

December 2017

Blank Page

APPROVAL PAGE

**COMPUTATIONAL AND EXPERIMENTAL DETERMINATION OF THE
MIXING EFFICIENCY OF A MICROFLUIDIC SERPENTINE
MICROMIXER**

Siril Arockiam

Dr. Piero M. Armenante, Thesis Advisor Date
Distinguished Professor of Chemical, Biological and Pharmaceutical Eng., NJIT

Dr. Sagnik Basuray, Thesis Co- Advisor Date
Assistant Professor of Chemical, Biological and Pharmaceutical Engineering, NJIT

Dr. Roman S. Voronov, Thesis Committee Member Date
Assistant Professor of Chemical, Biological and Pharmaceutical Engineering, NJIT

BIOGRAPHICAL SKETCH

Author: Siril Arockiam
Degree: Master of Science
Date: December 2017

Undergraduate and Graduate Education:

- Master of Science in Biopharmaceutical Engineering, New Jersey Institute of Technology, Newark, NJ, 2017
- Bachelor of Technology in Biotechnology, Anna University, Chennai, India, 2016

Major: Biopharmaceutical Engineering

I dedicate this thesis to Almighty and all my loved ones.

ACKNOWLEDGMENT

I would like to offer my heartfelt gratitude to my Thesis advisor, Dr. Piero M. Armenante and my Co-advisor Dr. Sagnik Basuray, who have provided support, encouragement and critique to complete my thesis steadily with valuable insights and proficient knowledge until the end of the thesis at the same time allowing me to perform with my independent approach.

I would like to thank my committee member Dr. Roman S. Voronov and for the time and I sincerely appreciate their support and their valuable feedback.

At last, I would like to thank my Family, Friends and Andrew, Mehnaz, Bhuvana, Roli and other Lab members who have supported me throughout the thesis.

TABLE OF CONTENTS

Chapter		Page
1	INTRODUCTION	
	1.1 Background Information.....	1
	1.1.1 Continuous Manufacturing of Pharmaceuticals	5
	1.1.2 Personalized Medicine.....	6
	1.1.3 COMSOL Multiphysics®.....	7
	1.2 Objectives.....	8
2	EXPERIMENTAL SYSTEM AND METHOD	
	2.1 Material.....	9
	2.1.1 Adhesive Tape.....	9
	2.1.2 Distilled Water.....	10
	2.1.3 Food Colorant.....	11
	2.1.4 Fluorescein Isothiocyanate (FITC).....	11
	2.2 Apparatus.....	12
	2.2.1 Cricut	12
	2.2.2 Syringe Pump	13
	2.2.3 Drill Machine	14
	2.2.4 Fluorescence Microscopy.....	14
	2.2.5 Digital Camera.....	16

TABLE OF CONTENTS

(Continued)

Chapter		Page
	2.3 Device Fabrication.....	17
	2.4 Experimental Method and Calculation.....	18
3	COMSOL	
	3.1 Assumptions and Initial Conditions.....	20
	3.2 Boundary Conditions.....	21
	3.3 Governing Equation.....	21
	3.4 Method of Solution.....	23
	3.5 Determination of Mixing Efficiency.....	25
4	RESULTS AND DISCUSSION.....	26
5	CONCLUSION.....	43
6	FUTURE WORK	44
	APPENDIX A COMSOL.....	45
	REFERENCES	52

LIST OF TABLES

Table		Page
1.1	Performance of Passive Micromixers in Recent Year.....	4
2.1	Specifications of Himamatsu Digital Camera	16
3.1	Values for Material Properties of Water	21
4.1	Parameters of Microchannel Dimension	30
4.2	Concentration and Intensity Values on Bend 2.....	31
4.3	Concentration and Intensity Values on Bend 4	32
4.4	Concentration and Intensity Values on Bend 6	33
4.5	Parameters of Microchannel Dimension.....	38
4.6	Values of Reynolds Number and Volume at Different Flow Rates.....	40
4.7	Mixing Efficiency of Simulation at 10 μ l/min.....	40
4.8	Mixing Efficiency of Simulation at 10 μ l/min.....	41

LIST OF FIGURES

Figure		Page
2.1	Adhesive tape.....	10
2.2	Milli-Q-Direct 16 system used to obtain deionized water.....	11
2.3	Food colorant.....	11
2.4	Cricut Explore® Machine.....	12
2.5	Programmable Syringe Pump.....	13
2.6	Drill machine for making inlet and outlet ports.....	14
2.7	Fluorescence microscope for taking images using FITC.....	15
2.8	FITC filter cube.....	15
2.9	Serpentine channel with T- shaped inlet from COMSOL.....	17
2.10	Microfluidic Device.....	18
3.1	Finite meshing of geometry.....	24
3.2	Corners of the microfluidic channel.....	25
4.1	Y-inlet straight channel.....	26
4.2	Y-inlet smooth edged serpentine channel.....	26
4.3	Y-inlet smooth edged and close by loop in serpentine channel.....	27
4.4	Fabricated Microfluidic device.....	27
4.4a	Fluorescent image near inlet at 10 μ l/min.....	28
4.4b	Fluorescent image at bend 2 at 10 μ l/min.....	28
4.4c	Fluorescent image at bend 4 at 10 μ l/min.....	29
4.4d	Fluorescent image at bend 6 at 10 μ l/min.....	29
4.5	Predicted oncentration profile at 10 μ l/min and the boxed region indicates the places where the fluorescent images have been taken and analyzed for intensity.....	30

LIST OF FIGURES

(CONTINUED)

4.6	Concentration Profile at Bend #2 at Flow Rate=10 μ l/min	32
4.7	Concentration Profile at Bend #4 at Flow Rate=10 μ l/min	33
4.8	Concentration Profile at Bend #6 at Flow Rate=10 μ l/min.....	34
4.9	Mixing efficiency at Flow rate=10 μ l/min.....	35
4.9a	Fluorescent image near inlet at 0.1 μ l/min	36
4.9b	Fluorescent image at bend 2 at 0.1 μ l/min	36
4.9c	Fluorescent image at bend 4 at 0.1 μ l/min	37
4.9d	Fluorescent image at bend 6 at 0.1 μ l/min.....	37
4.10	Concentration profile at Flow rate=0.1 μ l/min.....	38
4.11	Mixing efficiency at Flow rate= 0.1 μ l/min.....	39
4.12	Mixing efficiency of simulation at Flow rate=10 μ l/min.....	40
4.13	Mixing efficiency of simulation at Flow rate=0.1 μ l/min.....	41

CHAPTER 1

INTRODUCTION

1.1 Background Information

Microfluidics has opened up exciting new research areas in medical diagnostics, sensors, continuous manufacturing of pharmaceutical drugs [1]. Microfluidics offers the advantage of the increased surface area to volume ratios, thereby reducing the reagent or sample consumption and increasing surface reactions. Further microfluidic devices are compact and portable. All these factors lead to reduced cost of operation, production and the amount of sample. Microfluidic mixers find application in many biochemical processes such as the synthesis or sequencing of nucleic acids [2], DNA purification [3], chemical reactions [4] and polymerase chain reaction [5]. The additional advantage of integrating microfluidic mixers is a reduction in the incubation time for bead-based enzyme-linked immunosorbent assays (ELISA) used in the study of Immunological Assays.

However, when it comes to microfluidics, the huge disadvantage is its laminar flow profile. Due to the small channel dimension, the Reynolds Number is low. For example, the Reynolds number is of the order of 0.01 in a standard water-based microfluidic system with a channel width of $10\mu\text{m}$, a liquid flow rate of 1 mm/s , a fluid density of 1 g/cm^3 and a viscosity of 0.001 Ns/m^2 [6]. Because of this low Reynolds number regime, turbulent mixing does not occur, and hence diffusive mixing of species is dominant. However, diffusion is an inherently slow process. So the diffusion can be enhanced by external force or design of the device. Based on this, the mixing in the microfluidic mixers is classified as active or passive mixing.

Active mixing happens with the help of an external force; active mixing is implemented by integrating a mechanical transducer within the microfluidic device. Often this is achieved using microfabrication. For example, ultrasonic transducers that generate acoustic waves to stir the samples, have achieved increased mixing in a lower

time. However, these active transducers lead to significant heat generation, leading to an unwanted reaction.

Passive mixing is defined as once where the mixing is increased without the help of external transducer. Typically, this is achieved by increasing the contact area between the mixing species. A microfluidic channel architecture is designed that allows the species to interact and mix multiple times as they flow along the channel. There have been many studies in the literature on both active mixing and passive mixing in microfluidic geometry. In miniaturized flow systems with Reynolds numbers varying from 2 to 100, flow structures can be artificially induced, assisting flow segmentation through inertia effects. The majority of the 3D passive mixers [7-11] utilize multiple splitting, recombining, and rotating channels for the efficient mixing of fluids.

In lamination method, Buchegger *et al.* [12] proposed a horizontal multi-lamination micromixer based on wedge-shaped inlet channels. The experimental results revealed highly uniform fluid mixing in the low millisecond second range. Tofteberg *et al.* [13] fabricated a passive micromixer that made a controlled 900 rotations of a flow cross-section followed by a split into several channels the zigzag channel [14] considered in [15], segmentation was achieved through shear forces. Scampavia *et al.* [16] who fabricated a coaxial mixer containing an inner core liquid stream with a low flow rate and an outer flow stream with a higher flow rate demonstrated another example of mixing via inertia forces.

In the Zigzag model [17, 18] the species streams flowed close to the angled surface due to the Coanda effect, and this effect was used to guide the fluid streams to collide with one another. Mixing cells in opposite directions were then used to repeat the transverse dispersion caused by the flow impact. In the micromixer, one of the fluids was divided into two sub-streams, and one of these two sub-streams was then merged with the second fluid stream from the main channel in the micromixer.

Vijayendran *et al.* [7] [19] presented a three-dimensional serpentine [20-22] micromixer designed to induce a chaotic mixing effect. The mixing efficiency of the

serpentine microchannel was observed to be twice that obtained in a conventional straight microchannel. Liu *et al.* [23] considered a three-dimensional serpentine mixer, and a staggered herringbone mixer, and performed numerical simulations to investigate the mixing characteristics of the two devices for different Reynolds number regimes and fluorescent sample mass fractions. Jen *et al.* [24] presented a micromixer featuring a three-dimensional structure of twisted microchannels [20, 25-28] designed to induce a chaotic mixing effect within the fluid streams.

The twisted microchannels were designed such that the angle of the channels' lower surfaces alternated in each longitudinal subsection of the mixing channel. Hence, the fluid flow sways from side to side as it travels along the microchannel, resulting in a chaotic advection effect. Park *et al.* [27] presented a breakup method based on passive rotation for enhancing the mixing efficiency of micromixers. The proposed method not only actively generated interfaces between the mixing species but also enhanced the diffusion process at the interface. Hardt *et al.* [29] presented a low-Reynolds number split-and-recombine mixer. In their design, when fluid 1(2) entered the upper (lower) half of the stream, it was directed to the left (right) branch. The two streams were then recombined and directed into a channel with a cross-section identical to that of the inlet of the mixing element. In this way, the number of fluid lamellae doubled after each step, and the average lamella thickness halved.

Table 1.1 The Performance of Passive Micro Mixers in Recent Years.

Categorie s	Mixing Technique	Mixing Time (ms)	Mixing Length (μm)	Mixing Index	References
Laminatio n	Wedged shaped inlets	1	1	0.9	[12]
	90° rotation	-	-	0.95	[13]
Zigzag channels	Elliptic-shape barriers	-	10,000	0.96	[30]
3-D serpentine structure	Folding structure	489	-	0.01	[31]
	Creeping structure	-	-	0.015	[32]
	Multidirectional vortices	-	4255	0.72	[33]
Twisted channels	Split and recombine	730	96,000	~1	[34]
	T-/Y- mixer	-	1000	0.95	[21]

1.1.1 Continuous Manufacturing of Pharmaceuticals

Microreactors are a developing technology used to perform safer, more efficient, and more selective chemical transformations in microchannels or narrow-bore tubing [35-45]. These processes can be performed in lab-on-chip concept where the crystallization and preparation of zeolites have been already performed on microfluidic device [46, 47]. The many advantages associated with conducting reactions in flow are attributed to large surface-area-to-volume ratios [48] that allow precise reaction control through rapid heat transfer and mixing [49-52]. A major challenge facing the pharmaceutical industry is drug shortages; the U.S. Food and Drug Administration (FDA) has reported well over 200 cases per year during 2011–2014 [53]. The causes of these shortages often trace back to factors reflective of the limitations of batch-wise manufacturing, such as variations in quality control and supply chain interruption. Moreover, the small number of suppliers for any particular medicine further exacerbates the challenges faced by batch-wise manufacturing to respond to sudden changes in demand or need [54, 55]. Another major advantage of continuous manufacturing of pharmaceuticals in the microfluidic devices is the ability to produce personalized medicine focusing on particular need, which is not possible with the batch-wise production of bulk pharmaceuticals. Due to the cost efficiency in the construction of continuous manufacturing models in a microfluidic environment, it can be used in the production of personalized medicine.

1.1.2 Personalized Medicine

Personalized medicine has been defined by the American director of the Council for Science and Technology as “the adaptation of medical treatment to the individual characteristics of each patient, with the goal to classify individuals into subpopulations according to their susceptibility to disease or response to certain treatments [56]. Recent and rapid advances in genomics and molecular biology are revealing a growing number

of new genome-related molecular markers for the presence of the disease, susceptibility to disease or differential response to treatment. Use genome related markers as the basis of new genomics-based diagnostic tests for identifying or confirming the disease, assessing an individual's risk of disease, identifying patients who will benefit from particular interventions or tailoring dosing regimens to individual variations in metabolic response is now possible. This approach is also a good way for the development of new therapeutics specifically targeted at the physiological consequences of the genetic defect(s) associated with a patient's disease [56]. Its development in oncology requires a better understanding of mechanisms of carcinogenesis, identification of prognostic biomarkers and targeted therapies to assess the management of patients with a greater accuracy by using targeted and scientifically proven treatments. The traditional one-size-fits-all paradigm is going to be replaced by one that focuses on individualized patient care using specific genetic profiles and medical histories [57]. One of such applications of personalized medicine is a clinical diagnosis. Clinical diagnosis involving central facility and site visits can be a huge burden for patients with complex management, especially in resource-limited or rural areas. Point-of-care (POC) diagnosis has been an emerging field for advancing healthcare accessibility and affordability, which leads to faster results, timely interventions and excellent efficacy [58] Microfluidic lab-on-a-chip technology is a promising approach for POC diagnosis [59,60]. However, microfabrication of microfluidic devices always requires a scientific laboratory setting with expensive infrastructure. These can be overcome by adopting simpler techniques and using affordable materials for construction. For example, use of adhesive tapes for fabrication of microfluidic devices are cost-effective and easy to construct.

1.1.3 COMSOL Multiphysics®

COMSOL Multiphysics® is a general-purpose platform software for modeling engineering applications. COMSOL is a computational tool that employs numerical methods and algorithms to discretize and solve partial differential equations (PDEs) into solvable systems of equations to analyze fluid flow problems. Partial derivatives from the PDEs are replaced with finite difference quotients, which in turn are utilized to formulate difference equations. The difference equations are algebraic representations of the PDE and are solvable. In COMSOL, the object or system that is being studied is broken down into a finite number of cells. These cells are arranged throughout the geometry of the system and are commonly referred to as the mesh or the grid [61]. The difference quotients are replaced in the governing flow equations, creating systems of equations with dependent variables at each grid point within the mesh and a computer is used to solve the system. Numerical solutions of the equations are influenced mainly by two types of errors. The first type is discretization error, which is the difference between the exact solution of the PDE and the corresponding solution of the difference equation. This error is usually the cause of systems that fail to converge due to poorly defined boundary conditions. The second type is referred to as round-off error and is caused by calculations errors that originate from the solving computer.

1.2 Objectives

To design, experimentally test, and model a **simple, easy-to-build, cost-effective microfluidic device** that can be used to significant increase passive mixing in **micromixing** channels .This is done by doing various design of microfluidic channels and to find a microfluidic design that leads to significant increase in passive mixing in channels in terms of mixing efficiency. And to create a COMSOL model with necessary modules to simulate the hydrodynamics and the mixing process in the experiment and successfully extracting data from it. This will reduce the need for experimental runs. COMSOL simulations of mixing will be verified against experiments. The Microfluidic

mixer will be fabricated with Adhesive tape and Cricut, which is cost-effective, compared to the fabrication of channels by laser cutting. The mixing process will be studied by calculating the mixing efficiency in both experiments and COMSOL. The mixing efficiency will be obtained in the experiment by analyzing the fluorescent images obtained by using Fluorescein isothiocyanate (FITC) as a dye. In COMSOL, the slice plot of the concentration profile will be used to analyze the mixing efficiency along the cross-section of the channel. The parameters that will be varied in both experiments and simulation for increased mixing is:

- Design of Channel
- Channel Width
- Channel Depth
- Flow rate in the channel

Based on the results, definite conclusions can be drawn as to which parameter plays the most important role in the passive mixing. Experimental verification of simulation will help us to reinforce the results of increased passive mixing further.

CHAPTER 2

EXPERIMENTAL SYSTEM AND METHOD

2.1 Materials

In this experiment, to analyze the deionized mixing water is used. For visual analysis of mixing, food colorants are used as a dye in water. The other method used to analyze mixing is dissolving fluorophore in the deionized water. The fluorophore used in the experiment was Fluorescein isothiocyanate (FITC). The microfluidic device is fabricated using microscopic glass slides with the dimension 25mm ×75mm × 1mm with ground edges and 90°corners from Globe scientific Inc. The Adhesive tape held the device together and the channel design.

2.1.1 Adhesive Tape

ARcare® 90445(Ashesive Research Inc.) is a clear, thin and flexible plastic film coated on both sides with a medical grade pressure-sensitive adhesive. A clear polyester release liner on both sides protects the double-faced tape.

Features:

- Non-migratory acrylic adhesive
- Inert acrylic adhesive
- Easily die cut

Benefits:

- Allows lateral flow in membrane-based devices
- Compatible with many assays
- Facilitates design options

Profile and Diagram:

Substrate:	One mil clear polyester film
Adhesive:	AS-110 acrylic medical grade adhesive (both sides)
Liner:	2-mil clear polyester release film (both sides)
180° Peel Adhesion:	25 oz/in minimum (both sides)

Adhesive Thickness: 1.1 mils (both sides)

Thickness without Liners: 3.2 mils Total Thickness: 7.2 mils



Figure 2.1 Adhesive Tape.

Source: <http://www.adhesivesresearch.com/wp-content/uploads/2013/10/90445-Data-Sheet.pdf>

2.1.2 Distilled Water

The distilled water is produced by Milli-Q Direct 16 machine obtained from Millipore Sigma, which deionizes the water. The water used for the experiments was showing a conductivity of $7.3 \mu\text{S}/\text{cm}$ and having resistance of $12.4\text{M}\Omega\text{cm}$ was supplied from Milli-Q DI water system. The water was containing 2ppb of total organic carbon (TOC). The Milli-Q system used was shown in Figure 2.2.



Figure 2.2: Milli-Q-Direct 16 system used to obtain deionized water.

2.1.3 Food Colorant

The food colorant used were food grade colorants obtained from Badia Spices Inc., which are non-toxic and degradable dyes. The green and red food colorants were used. They were diluted with distilled water to make less concentrated by adding 5 drops for 10ml distilled water.



Figure 2.3 Food colorant.

2.1.4 Fluorescein Isothiocyanate (FITC)

Fluorescein isothiocyanate (FITC) was obtained from Sigma-Aldrich® (USA) for the experiment. Fluorescein isothiocyanate (FITC) is a widely used fluorophore for analysis under fluorescent microscope. It has molecular Formula of $C_{21}H_{11}NO_5S$, molecular weight of 389.4 Dalton. It has excitation at 495 nm and emission at 525 nm. 1mol/ml solution was prepared in distilled water by dissolving FITC in DI water. It was stored under refrigerated conditions.

2.2 Apparatus

The microfluidic device is constructed using Adhesive tape sandwiched between two glass slides. The apparatus such as Cricut, Drilling machine, Fluorescence Microscopy, Digital Camera were used.

2.2.1 Cricut

The Cricut Explore® device was used to fabricate/cut the adhesive tape in desired design. The design was created with Cricut interface. Cricut machine is easy enough to master by anyone. The adhesive tape will be stacked upon the mat for Cricut and loaded into the Cricut machine. The Cricut used the blade to cut the channels. Since the channel is complex and created on an adhesive tape, the settings on the Cricut were adjusted to vinyl. Because with other settings, either the tape will be damaged or the cut would not be deep enough to penetrate both liner and adhesive part. Even with the Vinyl settings, three consecutive cuts was made to have enough penetration through the tape.



Figure 2.4 Cricut Explore® Machine.

2.2.2 Syringe Pump

In this experiment, New Era NE-1000 Programmable single channel syringe pump from New Era Pump Systems Inc. was used. To have a regulated flow rate, the syringe pump was used. The flow rates were varied between 0.01 μ l-10 μ l. 3ml BD (USA) syringe with inner diameter of 8.42mm was used. The inner diameter of the syringe was entered as 8.42 mm in the syringe pump for automatic calibration of the pump for desired flow rate. The Saint Gobain- Tygan-S™ tubings were used to connect the syringe and the microfluidic device. The fluid ports were attached to both the side of the tubing to facilitate the flow. The syringe was held in one place by placing it between the clamps, which hold the syringe firmly in the pump. The flow rate can be entered through the digital input. The syringe was prefilled with food colorant mixed water.



Figure 2.5 Programmable Syringe Pump.

2.2.3 Drill Machine

Central Machinery® 5 speed drill press of model 38119 was used with input voltage of 120Volt. The drill chuck capacity is 1/2 inch and the maximum distance from chuck to table is 6-3/4 inch. The 1mm drill bit was used to drill hole on the glass slides. The position of drilling on glass slide is based on the specifications of channel. The Figure 2.6 shows the drill machine used for making inlet and outlet ports in glass slide.



Figure 2.6 Drill machine for making inlet and outlet ports.

2.2.4 Fluorescence Microscopy

The Olympus BX-51 fluorescence microscope from Spectra Services was used in the lab. It uses UIS2 optical system with vertical movement of stage up to 25mm, high sensitivity in focusing knob was observed. It has built-in Koehler illumination for transmitted light 12V100W halogen bulb. Light preset switch with light intensity LED indicator is present. The Figure 2.7 shows the fluorescence microscope.

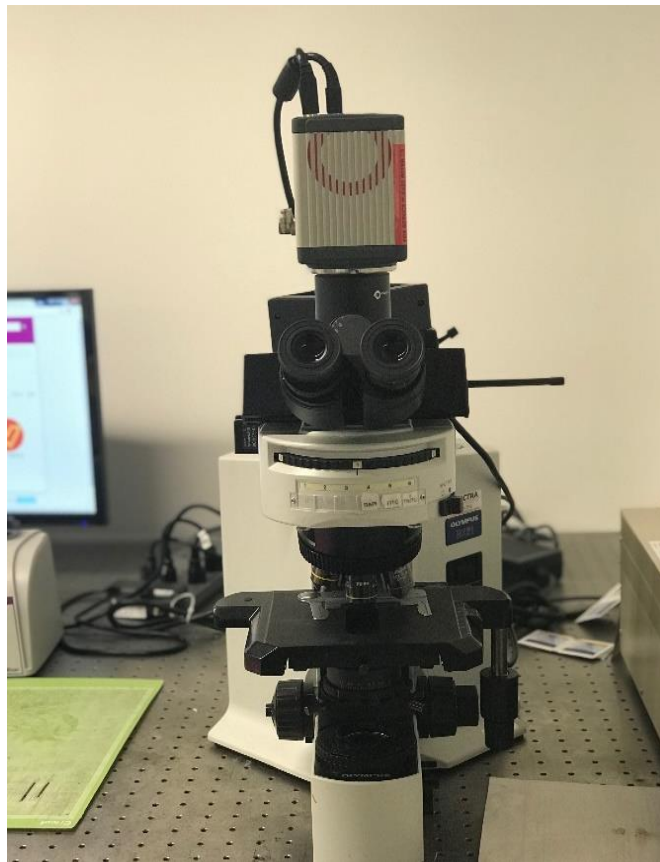


Figure 2.7 Fluorescence microscope for taking images using FITC.

The UV light was used for the fluorescence microscope. FITC filter cube was used since FITC dye was used to visualize the flow profile. The Figure 2.8 gives the diagrammatic representation of the FITC filter cube.

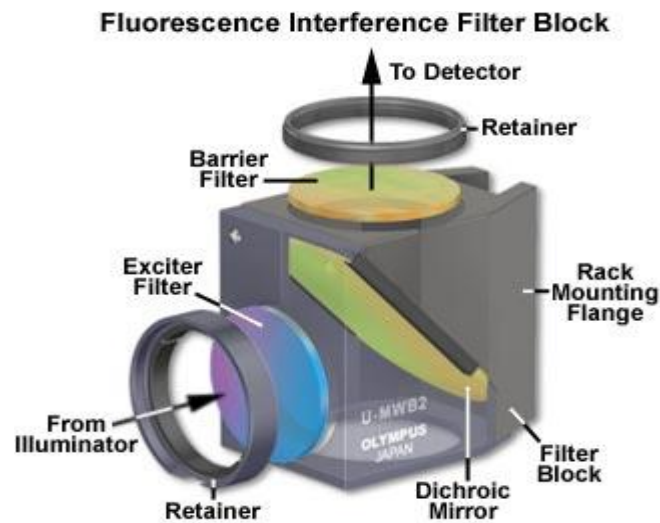


Figure 2.8 FITC filter cube.

Source: <https://www.olympus-lifescience.com/es/microscope>

resource/primer/techniques/fluorescence/filters/

Exciter filters permit only selected wavelengths (467 – 498nm) from the illuminator to pass through on the way toward the specimen. Dichromatic beamsplitters (dichroic mirrors) are specialized filters, which are designed to efficiently reflect excitation wavelengths and pass emission wavelengths. They are used in reflected light fluorescence illuminators and are positioned in the light path after the exciter filter but before the barrier filter. Dichromatic beamsplitters are oriented at a 45-degree angle to the light passing through the excitation filter and at a 45-degree angle to the barrier filter as illustrated in Figure 2.8. Barrier filters are filters, which are needed to suppress or block (absorb) the excitation wavelengths and permit only selected emission wavelengths (513 – 556nm) to pass toward the eyepiece or camera.

2.2.5 Digital Camera

The Hamamatsu Digital Camera C11440 with ORCA-flash4.0 was used to take images. The 16 -Bit black and white images were taken for the better gray scale value, which will be helpful in the intensity analysis. The exposure time of the camera was set to 100ms. The specifications of the camera are listed in table 2.1

Table 2.1: Specifications of Himamatsu Digital Camera

Imaging Device	Scientific CMOS image sensor
Effective number of pixels	2048(H)×2048(V)
Cell size	6.5μm(H)× 6.5μm(V)
Effective area	13.3mm×13.3mm
Full well capacity	30000 electrons

2.3 Device Fabrication

The microfluidic device is designed in the serpentine model; this will lead to more contact time and Surface contact between species within the small length of the device. The inlets can be either T or Y shaped. The channel geometry is shown in Figure 2.9.

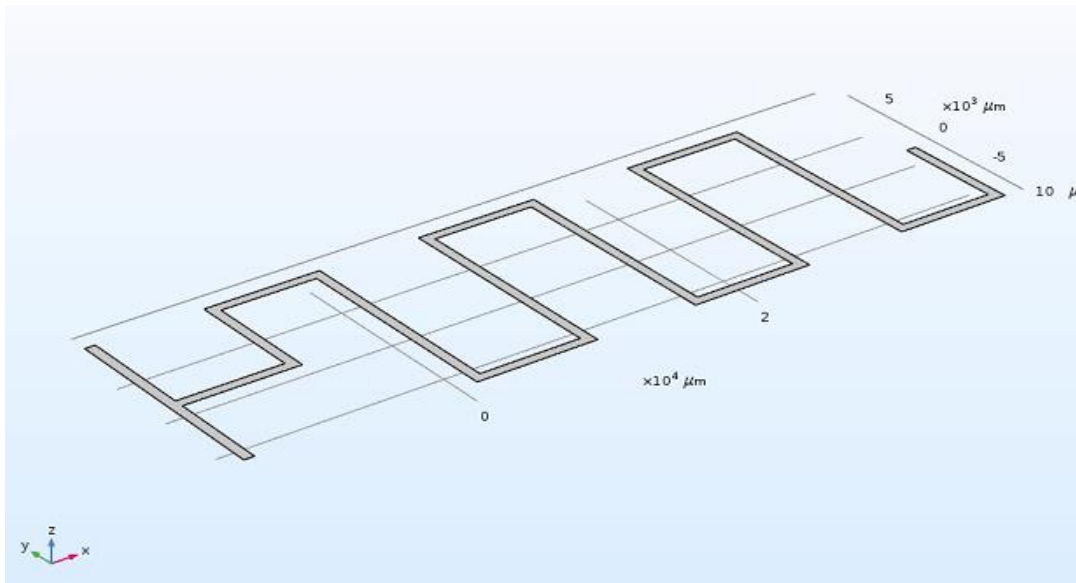


Figure 2.9 Serpentine channel with T- shaped inlet from COMSOL.

Glass slides of 5x75x1mm with ground edges and 90° corners were used to construct the device. The glass slides were cleaned with the Acetone, then the double sided adhesive tape which is been fabricated with the desired design was adhered to the glass slide after it is aligned with the corners. Then the adhesive tape was pressed hard to remove the air bubbles between the glass slide and the tape. Then the second glass slide was drilled with inlet and outlet holes and then been aligned with the fabricated channels inlet and outlet. After that the glass slide was adhered on top othe tape, again it was pressed to remove the air bubbles. Later, the fluid ports were glued to the inlet and outlet holes and had been left to dry for some time. The diagrammatic representation of the microfluidic device can be observed in Figure 2.10

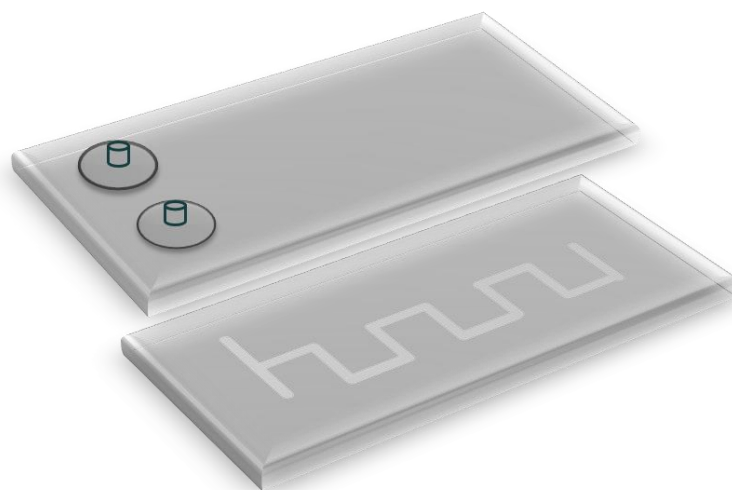


Figure 2.10 Microfluidic Device.

Table 2.2 Specifications of Device

Depth of the Channel	25 μ m
Width of the Channel	700 μ m
Length of long arm	15 μ m
Length of short arm	7.5 μ m
Total length	157.5 μ m
Total volume	2.75 μ l/min

e

2.4 Experimental Method and Calculation

The two inlet channels in the microfluidic device were connected to two syringes mounted in the syringe pump. The first channel was fed with the first syringe containing distilled water. The second channel was fed with a Fluorescein Isothiocyanate (FITC) solution (1 millimolar). The device was placed under the fluorescence microscope and focused at 4X magnification. The desired flow rate was programmed into the syringe pump. The pump was started and the fluids were fed to the channels. Once steady state was reached, images were captured at different locations in the mixing device with constant exposure time set at 100ms. Images were analyzed to determine the light intensity in each of the regions of interest with constant area in order to quantify the distribution of the tracer across selected cross sections along the channels. Calibration curves were obtained to quantify the FITC concentration from the intensity of the fluorescent light in images

The equations were obtained concerning previously published articles [62, 63]. The pixel densities were obtained using the ImageJ software, with the pixel intensity weight for the gray scale value at 16 Bit-image. The local mixing efficiency, σ_i at each point i on a selected cross section in the device was then determined from Equation 2.1. The intensity obtained from ImageJ was introduced into Equation 2.2 to calculate the mixing efficiency of the device. The concentration profile along the width of the channel and increase of the mixing efficiency with the number of mixer units was then determined.

An optical method was used for testing the efficiency of the mixer. The mixing pictures were recorded using a Hamamatsu digital camera that captured 3D devices in a single focused fluorescent image. The mixing efficiency was measured by

$$\sigma = 1 - \sqrt{\frac{1}{N} \sum_{i=1}^N (\sigma_i)^2}, \quad (2.1)$$

where σ_i is the total deviation at pixel i

$$\sigma_i = \frac{(I_i - I_{mix})}{(I_{unmix} - I_{mix})}, \quad (2.2)$$

I_i is the pixel intensity of the pixel i , I_{unmix} is the intensity prior to mixing, and I_{mix} is the intensity after complete mixing has been achieved (typically 0.5).

At steady state, the mixing intensity at any specific cross section does not vary with time. By determining the mixing intensity at different cross sections along the device, it is possible to follow the progress of the mixing process along the channel. The mixing intensity, and especially the mixing intensity at the end of the device, can provide quantitative information on the mixing performance of the device itself. The mixing intensity can be obtained as a function of a number of operating parameters (e.g., overall flow rate, channel length, channel width, etc.)

CHAPTER 3

COMSOL

The microfluidic device model was set up in COMSOL Multiphysics 5.3 and simulated in it using a computer with the following configuration: Intel(R) Xenon(R) CPU E5-2640 @ 2.50GHz(2 processors), 128 GB RAM, 64 bit Windows 10.

The single-phase laminar forced convective flow of water in a T shaped inlet microchannel with the transport of diluted species is simulated. The diffusive mass transport of a diluted Species (solute species) will set up concentration gradients in the channel. However, the fluid motion allows a convective term, which can significantly modify the concentration gradient of the chemical species. Hence, the transport process to be simulated here must take into account diffusion, dispersion, and convection. For a laminar fluid flow at steady state, streamlines that follow the velocity field do not cross each other. Since convection transports mass only tangent to the velocity, it cannot lead to mass transfer between adjacent layers of fluid. For a laminar flow at steady state, the only diffusion can allow mass transfer normal to the fluid flow. The objective of this study is to observe the parameters at which efficient mixing have achieved. The following sections will focus on the assumptions, initial conditions, boundary conditions, governing equations and steps in COMSOL for setting up the model for simulating the laminar flow coupled with mass transfer in the microchannel.

3.1 Assumptions and Initial Conditions

Several assumptions are made for this model including constant properties, no gravitational forces, incompressible fluid [64], and smooth surfaces of the channel, no-slip conditions [65-67], no total flux, and constant initial concentration in the system [68]. An initial condition was set that the initial concentration is zero across the system. The material in the system is water, and the material property is set to water. Gravitational forces are neglected since the system is horizontal and that the static

pressure under gravity is very low ($P = \rho gh$; $1000\text{kg/m}^3 * 9.81\text{m/s}^2 * 100\mu\text{m} = 0.9\text{ Pa}$). Tretheway and Meinhart (2002) [69] have shown using particle image velocimetry that the no-slip condition is valid for water flowing through hydrophilic channels. The following are the initial conditions and material properties given for the model:

$T=300\text{ K}$, $p = 0\text{ Pa}$, $u = 0\text{ m/s}$ similar to the initial conditions taken in (Liu & Garimella, 2005)'s work [67].

Table 3.1 Values for the Material Properties of Water

Property	Name	Value	Unit
Dynamic viscosity	μ	0.0008509	$\text{Pa}\cdot\text{s}$
Ratio of specific heats	γ	1.0	1
Heat capacity at constant pressure	C_p	0.00418	$\text{J}/(\text{kg}\cdot\text{K})$
Density	ρ	996.59	Kg/m^3
Thermal conductivity	k	0.6	$\text{W}/(\text{m}\cdot\text{K})$

3.2 Boundary Conditions

Boundary conditions are chosen to solve the laminar flow and transport profiles. For the laminar flow profile, the inlet velocity is set as 10^{-6} and 10^{-5} m/s . The outlet pressure is set at $p = 0\text{ Pa}$ since the pressure at the outlet is equal to atmospheric pressure. Additionally, the walls have the ideal no-slip condition. For the transport of diluted species profile, the inlet concentration is set at $1\text{ mol}/\text{m}^3$. The outflow area is also set where diffusion is zero. The diffusion coefficient of the system is set at $1 * 10^{-9}\text{ m}^2/\text{s}$. The concentration at inlet 1 is considered as $1\text{ mol}/\text{m}^3$ and at inlet 2 as 0.

3.3 Governing Equations

The Navier-Stokes equation governs fluid dynamics. The conservation of momentum is represented by Navier-Stokes equation whereas the continuity equation represents the conservation of mass. Equation 4.1 accounts for the case of a compressible Newtonian fluid, where p is fluid pressure, u is the velocity of the fluid, ρ the fluid

density and μ the fluid dynamic viscosity. The first term on the right-hand side is the viscous force, while the second term represents the incompressible viscous fluid (stress constitutive). The first term on the left-hand side of equation 3.1 is the inertial force. Finally, the third term represents the external forces applied to the fluid.

$$\rho \left(\frac{\partial \mathbf{u}}{\partial t} + \mathbf{u} \cdot \nabla \mathbf{u} \right) = -\nabla p + \nabla \cdot \left(\mu (\nabla \mathbf{u} + (\nabla \mathbf{u})^T) - \frac{2}{3} \mu (\nabla \cdot \mathbf{u}) \mathbf{I} \right) + \mathbf{F} \quad (3.1)$$

The Navier-Stokes equation is solved along with the continuity equation from equation 3.2:

$$\frac{\partial \rho}{\partial t} + \nabla \cdot (\rho \mathbf{u}) = 0 \quad (3.2)$$

These equations can be simplified. In fluid dynamics, flow regimes are classified using a non-dimensional number, such as the Reynolds number. The Reynolds number is the ratio of inertial forces to viscous forces, $Re = \rho UL/\mu$. In this study, the flow is laminar and incompressible. Therefore, the continuity equation (Eq 3.2) reduces to equation 3.3.

$$\nabla \cdot \mathbf{u} = 0 \quad (3.3)$$

The term $(-\frac{2}{3}\mu(\nabla \mathbf{u})\mathbf{I})$ is also equal to zero and can be removed from the viscous force term in the Navier Stokes equation as the divergence of the velocity is equal to zero for incompressible fluids in Eq 3.3. Additionally, since gravity forces are neglected, the external forces term, 'F', is also removed from the Navier Stokes equation. Finally, the Navier Stokes equation reduces to equation 3.4.

$$0 = -\nabla p + \nabla \cdot \left(\mu (\nabla \mathbf{u} + (\nabla \mathbf{u})^T) \right) \quad (3.4)$$

$$\frac{\partial C_i}{\partial t} + \nabla \cdot D_i \nabla C_i + \mathbf{u} \cdot \nabla C_i = R_i ; \mathbf{N}_i = -D_i \nabla C_i + \mathbf{u} C_i \quad (3.5)$$

The mass equation is given by equation 3.5. C_i is the concentration of the species of interest, in the mass transfer equation 3.5. D_i is the diffusivity term, \mathbf{u} is average velocity, and R_i describes "sources" or "sinks" of the quantity C_i . The first term on the left-hand side represents the mass accumulation term, the second term on the left-hand side represents diffusion, and the third term represents convection (or advection). The term on the left-hand side, R_i , describes the growth or consumption through a possible

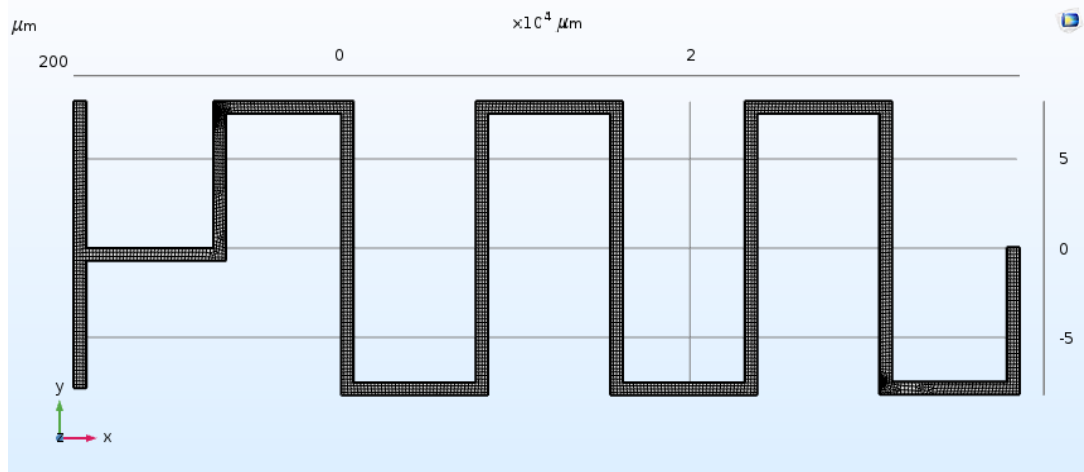
reaction. The second equation represents the total flux N_i , which is a summation of the diffusion and convective flux. The Navier Stokes equations from fluid dynamics need to be solved together with the mass transport equation. There are four unknowns (dependent variables), namely, the velocity field components, u and v , the pressure and the concentration. The equations are related through bidirectional Multiphysics couplings. It involves fluid dynamics coupled with mass transport. The pressure p and the velocity fields u and v are solutions of the Navier Stokes equations whereas the concentration c is solved using the mass transport equation. The equations are solved here using a finite element method called COMSOL. COMSOL solves them using stationary solvers for a particular set of boundary conditions and predicts the above unknown variables for a given geometry.

3.4 Method of Solution

For an accurate representation of the model, a geometric model is set up. Then, the relevant physics is chosen in COMSOL Multiphysics 5.1. The single-phase laminar flow and transport in diluted species physics are selected along with a stationary study. The geometry was manually built in COMSOL. Two inlets and one outlet hole are created, connecting to the microchannel. The microchannel is $700\mu\text{m}$ (W) x $25\mu\text{m}$ (D). Further, unlike other 2D studies, a 3D geometry is chosen here which significantly complicates the simulation (specifically the finite element mesh). The next step in creating geometry is to add material. Water is added to all the domains of the geometry. The Laminar flow physics node is then selected and the appropriate boundary conditions provided. The inlet velocity is mentioned after selecting the respective boundary in the geometry. Likewise, the outlet pressure condition ($p = 0 \text{ Pa}$) is given to the outlet boundary. No-slip boundary conditions are provided on all solid interfaces, and the initial conditions are set to zero. For the Transport in Diluted Species physics, a similar process is followed. The concentration of the species is initially set at zero. An inlet concentration is set at 1 mol/m^3 . The outflow area is also set where diffusion

is zero. The diffusion coefficient of the system is configured at $1 * 10^{-9} \text{m}^2/\text{s}$. The mass transport in fluids and laminar flow physics are coupled by selecting the Multiphysics coupling node. COMSOL is based on the finite element method approach. This necessitates choosing an appropriate mesh as COMSOL discretizes the model and in the process divides into many nodal elements. The processing phase solves equations for these nodes and obtains results. In this study, a user-defined mesh/selective mesh is selected for this geometry as shown in Figure 3.1

Figure 3.1 Finite meshing of geometry.



For more accurate computational results, the corner refinement has been used as shown in Figure 3.2. The mesh is selected as a finite element because the depth of the channel is $25 \mu\text{m}$, which is much smaller than coarse element size.

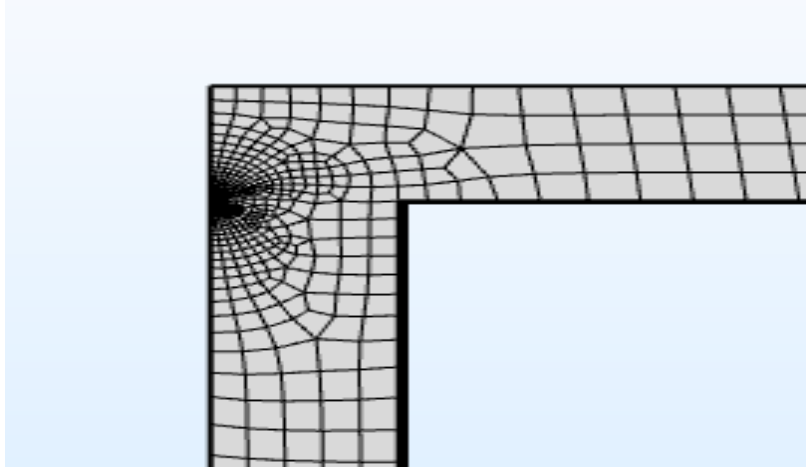


Figure 3.2 Corners of the microfluidic channel

3.5 Determination of Mixing Efficiency

The slice plots were obtained from COMSOL and the data was extracted into Excel. The local mixing efficiency, σ_i at each coordinate (x,y,z) i on a selected slice plot from the COMSOL was then determined from:

$$\sigma_i = \frac{C_i - C_{mix}}{C_{unmix} - C_{mix}} \quad (3.6)$$

C_i is the concentration at coordinate i , C_{unmix} is the concentration prior to mixing, and C_{mix} is the concentration after complete mixing has been achieved (typically 0.5). The mixing intensity σ for a selected cross section in the device was then determined from the local mixing intensities σ_i of all coordinates along that cross section of slice plot:

$$\sigma_i = \frac{(I_i - I_{mix})}{(I_{unmix} - I_{mix})}, \quad (3.7)$$

CHAPTER 4

RESULTS AND DISCUSSION

The microfluidic device fabrication can be made simple on adhesive tape and glass slide using Cricut, the parameters such as the number of repeated cuts and the pressure played a major role in obtaining clear-cut. The vinyl cutting settings were used. Figure 4.1 shows the fabricated microfluidic device.

In order to find an effective design various design have been tried during the initial stages of experiment, After the extensive the sharp edges with T-inlet gave some extent of mixing when observed visually.

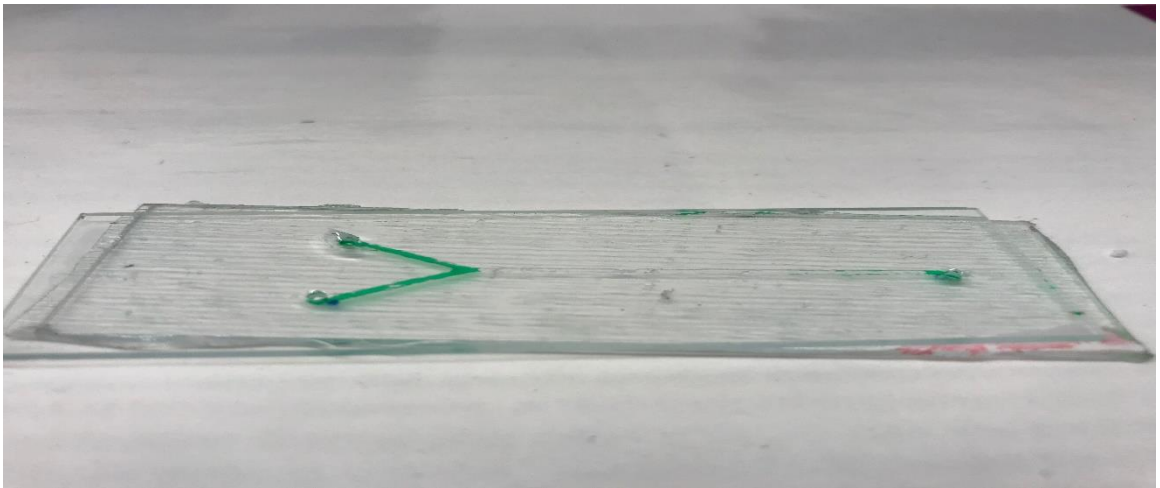


Figure 4.1 Y-inlet straight channel.

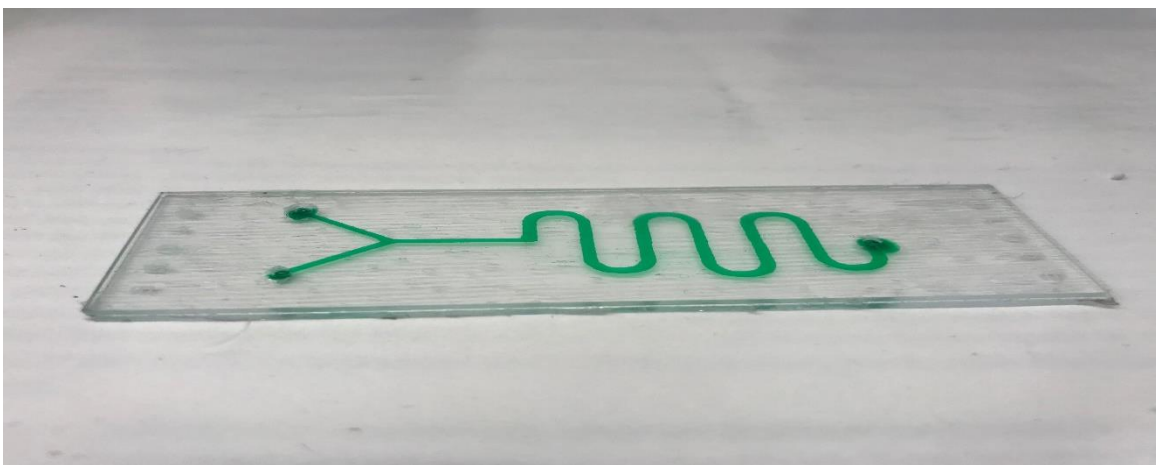


Figure 4.2 Y-inlet smooth edged serpentine channel.

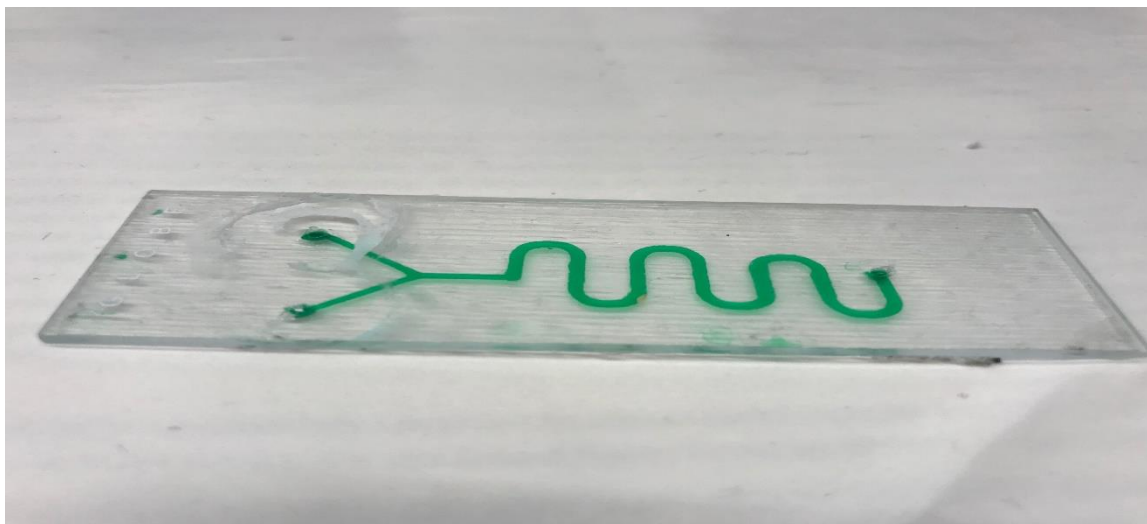


Figure 4.2 Y-inlet smooth edged and close by loop in serpentine channel.

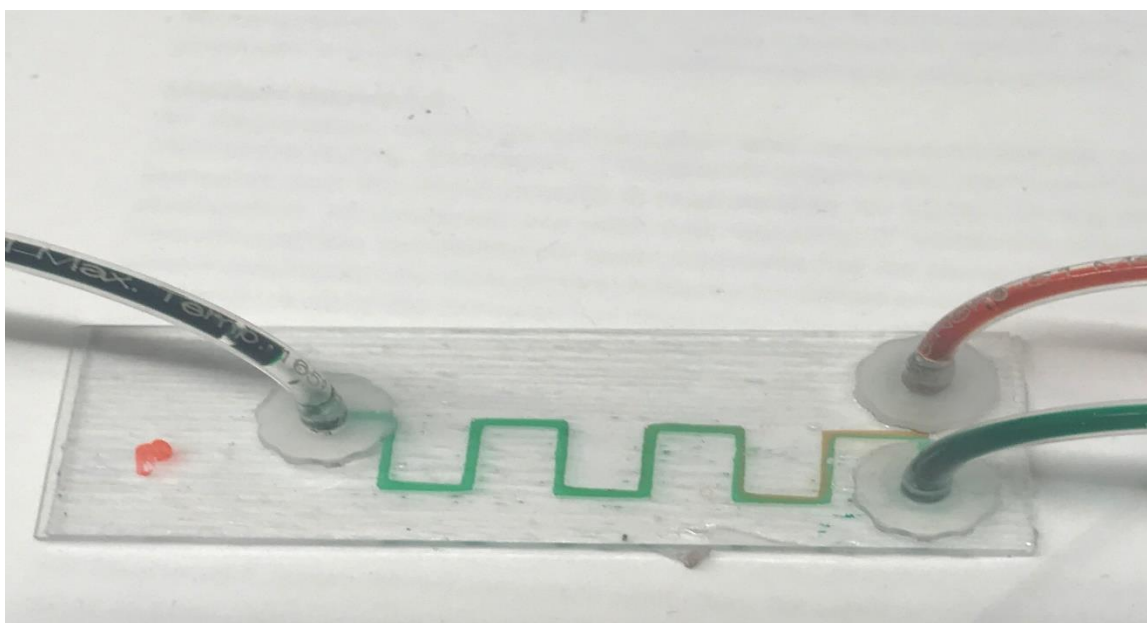


Figure 4.1 Fabricated microfluidic device.

However, to observe Mixing, the Fluorescein isothiocyanate (FITC) fluorescent dye at 1 Millimolar concentration was used as mixing dynamics cannot be quantified using food coloring. The experiment was conducted at $10\mu\text{l/ml}$ and $0.1\mu\text{l/ml}$. The Figure 4.2a is the fluorescent image taken near inlet at the flow rate of $10\mu\text{l/ml}$, and the Figure 4.2b is the fluorescent image taken at the bend 2, and Figure 4.2c is taken at the bend 4, and Figure 4.3 is the fluorescent image at the bend 6. The bright field indicates the flow of dye mixed DI water and the dark region indicates the flow of the blank DI

water. The channels have been highlighted with yellow dotted lines to know the boundary of channels.

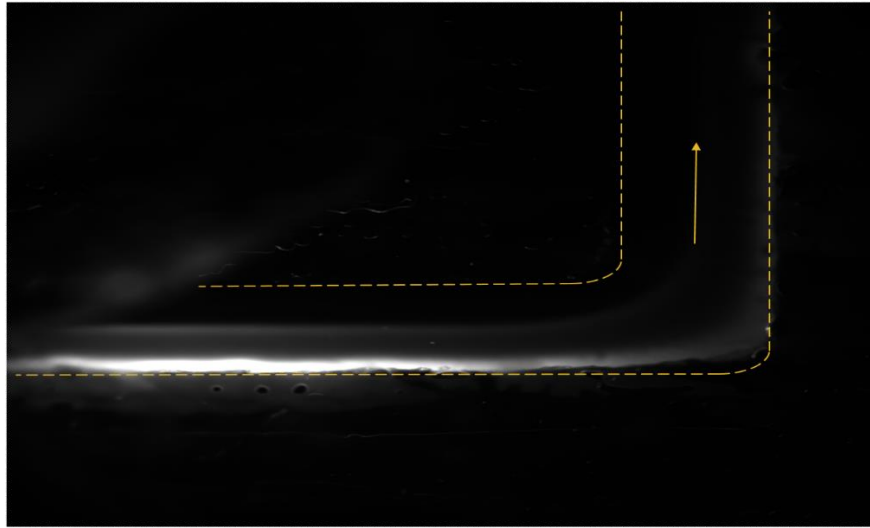


Figure 4.2a Fluorescent image near inlet at 10 μ l/min.

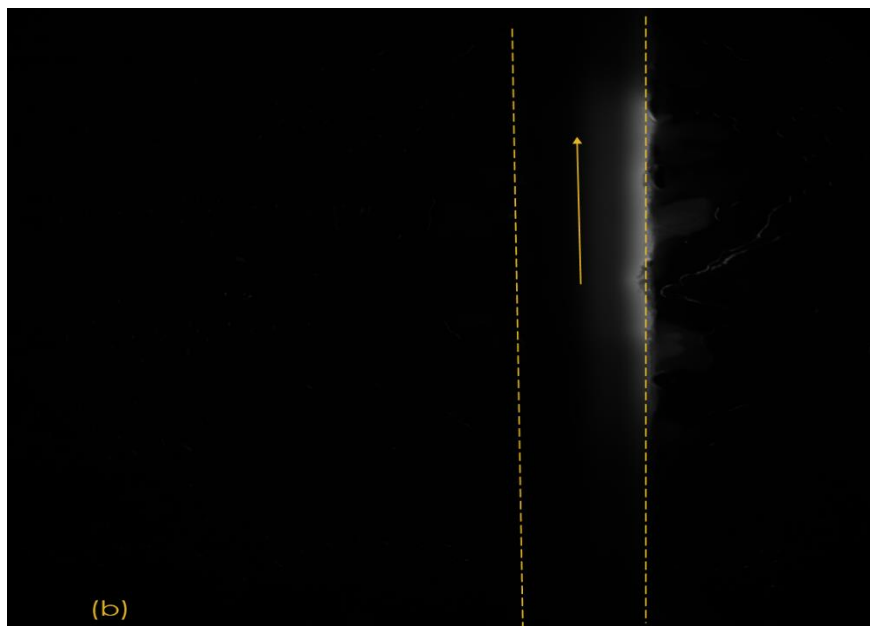


Figure 4.2b Fluorescent image of bend 2 at 10 μ l/min.

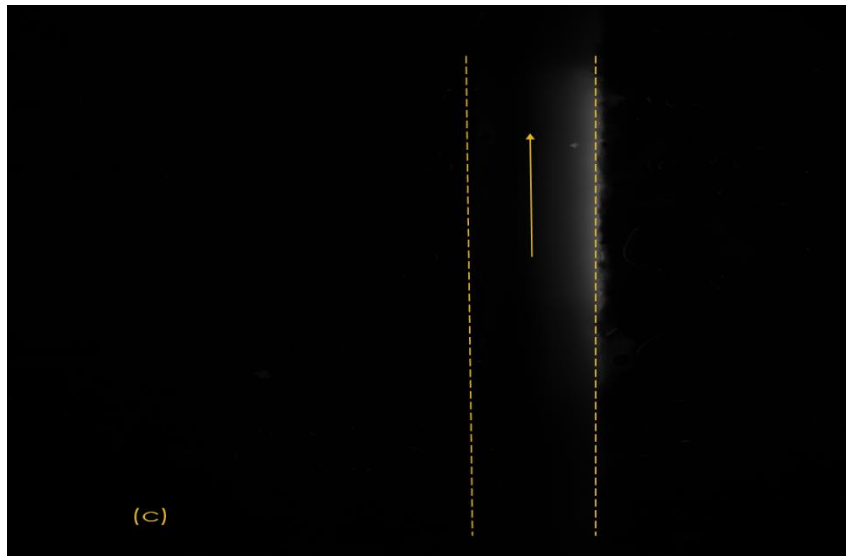


Figure 4.2c Fluorescent image of bend 4 at 10 μ l/min.

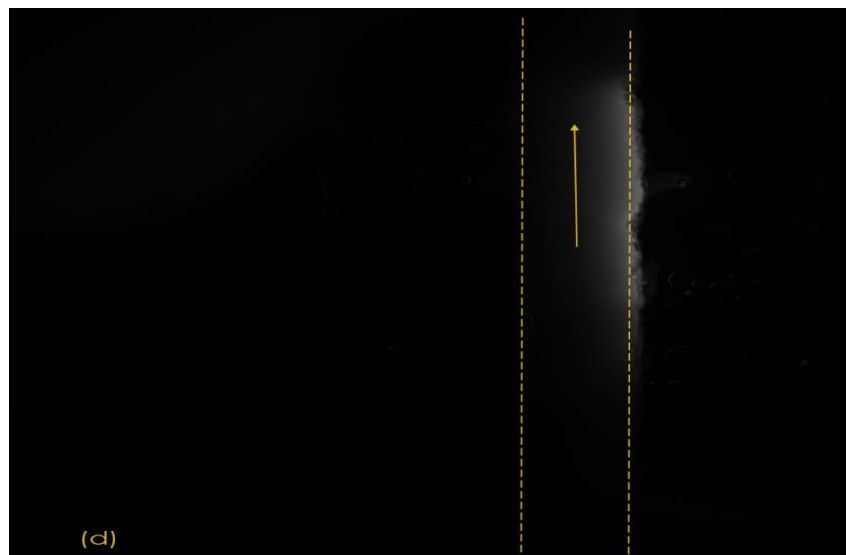


Figure 4.2d Fluorescent image of bend 6 at 10 μ l/min.

From the above Figures its visible that the dye is getting diffused from one stream to another stream. In Figure 4.2a, both the streams are maintaining the distinctive flow, but with the progress of bend, bright region in the image is slightly moving towards the left side from the right side as an indication of diffusion. But, to signify the mixing the entire channel should be observed as a bright region.

The simulation for this flow is done at same parameters to verify the results which are done both in simulation and experiment are agreeing up.

Table 4.1 Parameters of Microchannel Dimension

PARAMETERS	Value
Width of the channel	700 μm
Depth of the channel	25 μm
Number of Loops	3
Flow Rate	0.1 $\mu\text{l}/\text{min}$

Figure 4.3 is the concentration profile obtained from the COMSOL simulation for flow rate at 10 $\mu\text{l}/\text{min}$. The concentration profile is agreeing up with the experimental profile based on visual observation.

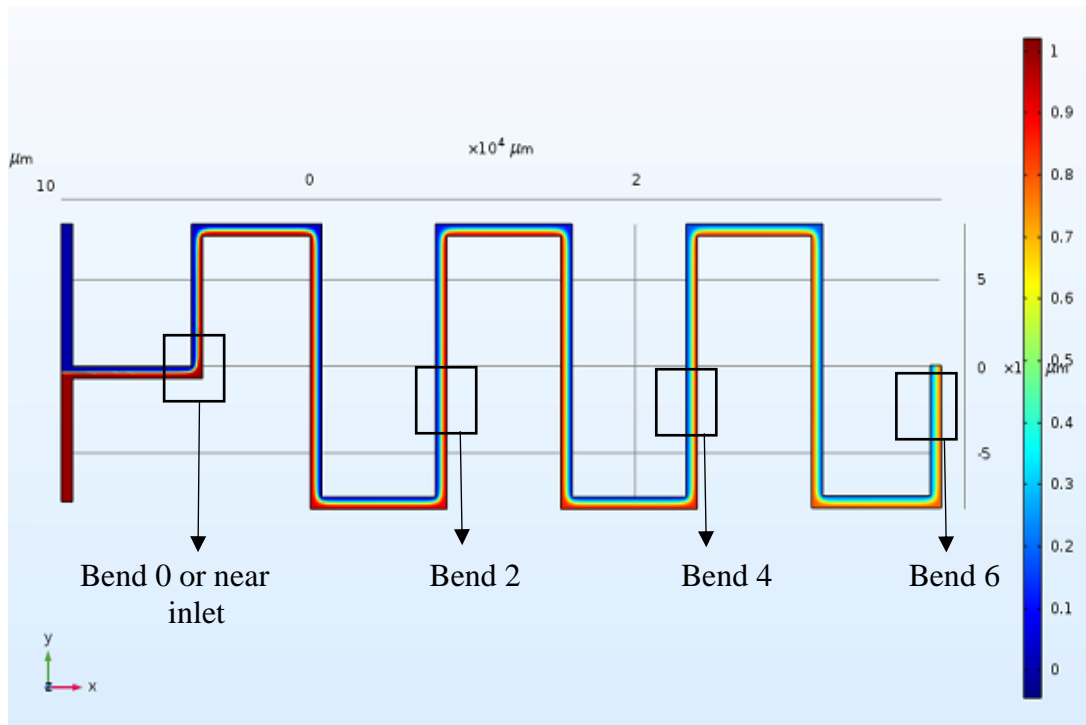


Figure 4.3 Predicted concentration profile at Flow rate= 10 $\mu\text{l}/\text{min}$ and the boxed region indicates the places where the fluorescent images have been taken and analyzed for intensity.

In the COMSOL, results the red color indicates the molecules and the blue color indicates the blank region. As the bend progress, the red color is shifting to the blue

color region slowly along the center indicating the diffusion of molecules from one stream to other.

To quantify the mixing, the concentration profiles are evaluated along the arc length at the end one point in each bend in COMSOL and experiment. The concentration profile has been obtained from the fluorescent images regarding intensity values using ImageJ software.

TABLE 4.2 Concentration and Intensity Values on Bend 2

Width of the channel(X-axis×100μm)	Concentration value from COMSOL	Intensity Value from Experiment
0	0.90593	0.90322
1	0.90592	0.90848
2	0.83562	0.79463
3	0.6419	0.59172
4	0.38193	0.30512
5	0.12488	0.15514
6	0.05039	0.0448
7	0.05026	0.01487

These values have been plotted as a graph to know the similarity between the COMSOL and Experiment. Figure 4.4 is the graph for the concentration profile for the Bend 2 which is observed at 10μl/min.

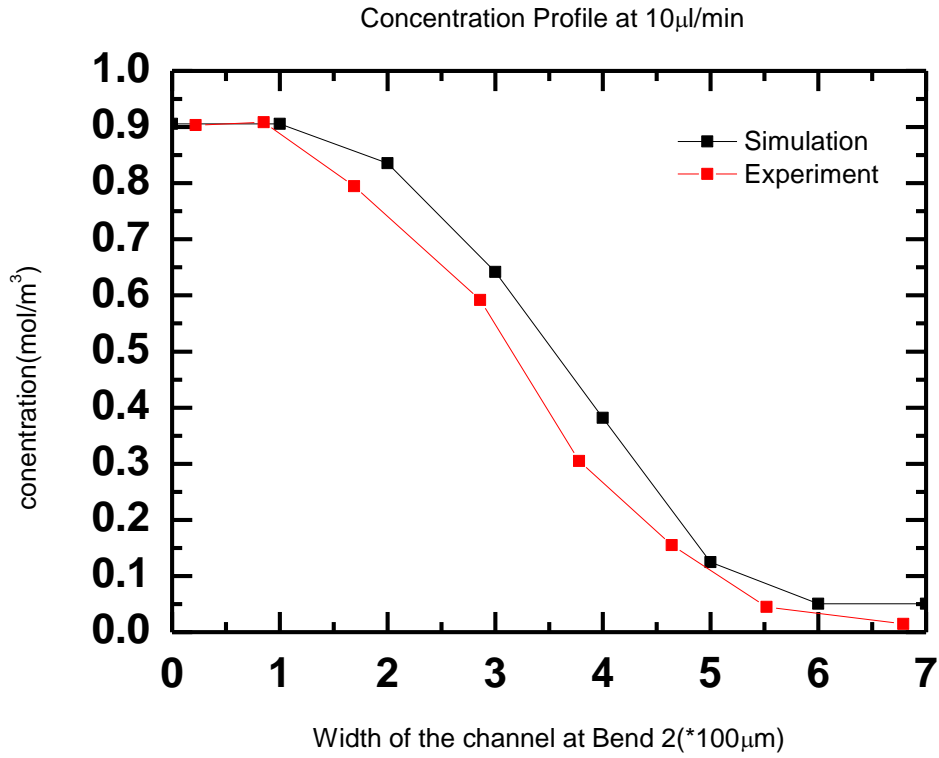


Figure 4.4 Concentration Profile at Bend #2 at Flow Rate=10 μ l/min.

The concentration profile obtained along the bend 4 at 10 μ l/min have been tabulated below.

Table 4.3 Concentration and Intensity Values on Bend 4

Width of the channel(X-axis \times 100 μ m)	Concentration value from COMSOL	Intensity Value from Experiment
0	0.80666	0.83971
1	0.79012	0.79413
2	0.71071	0.68229
3	0.5415	0.54567
4	0.33864	0.331
5	0.22486	0.25109
6	0.17689	0.22241
7	0.17047	0.18955

These values have been plotted as a graph to know the similarity between the COMSOL and Experiment. Figure 4.5 is the graph for the concentration profile for the Bend 4 which is observed at 10 μ l/ min.

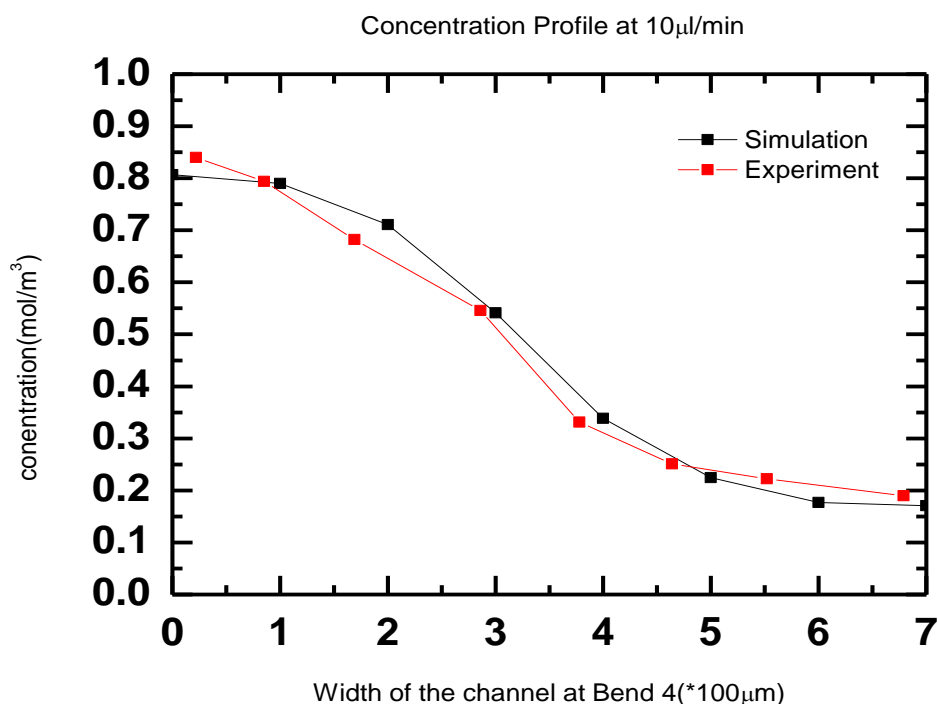


Figure 4.5 Concentration Profile at Bend #4 at Flow Rate=10 μ l/min.

Again, the concentration profile obtained along the bend 6 at 10 μ l/min have been tabulated below.

Table 4.4 Concentration and Intensity Values on Bend 6

Width of the channel(X-axis \times 100 μ m)	Concentration value from COMSOL	Intensity Value from Experiment
0	0.7265	0.76295
1	0.70837	0.71615
2	0.65744	0.63254
3	0.53953	0.52745
4	0.35514	0.34371
5	0.28429	0.2621
6	0.2658	0.23257
7	0.26122	0.16965

Once again these values have been plotted as a graph to know the similarity between the COMSOL and Experiment. Figure 4.6 is the graph for the concentration profile for the Bend 6 which is observed at $10\mu\text{l}/\text{min}$.

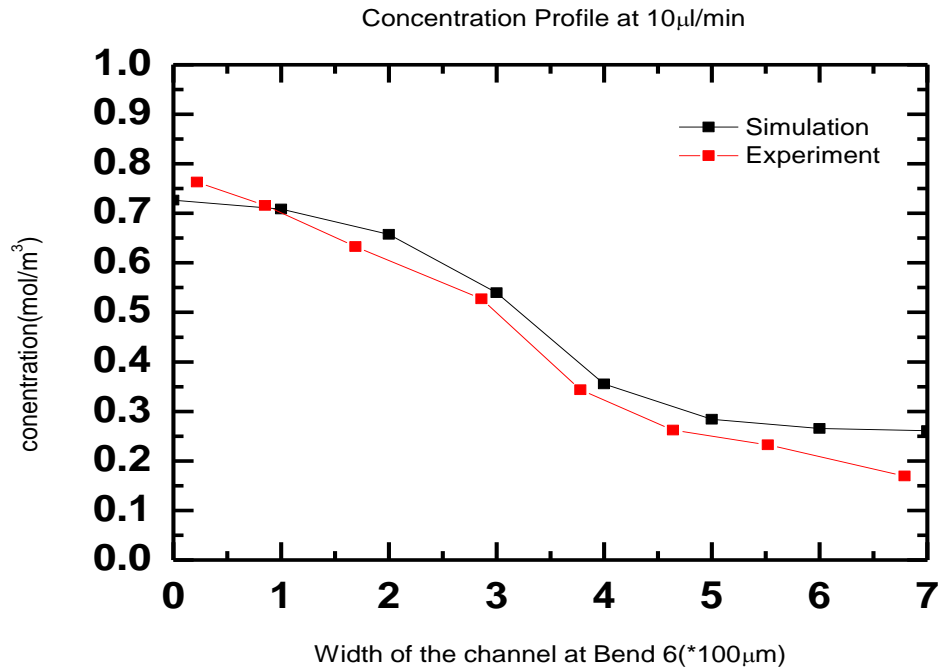


Figure 4.6 Concentration Profile at Bend #6 at Flow Rate= $10\mu\text{l}/\text{min}$.

The concentration values obtained along the bends are used to find the mixing efficiency at each bend at a flow rate of $10\mu\text{l}/\text{min}$ and have been plotted as a graph.

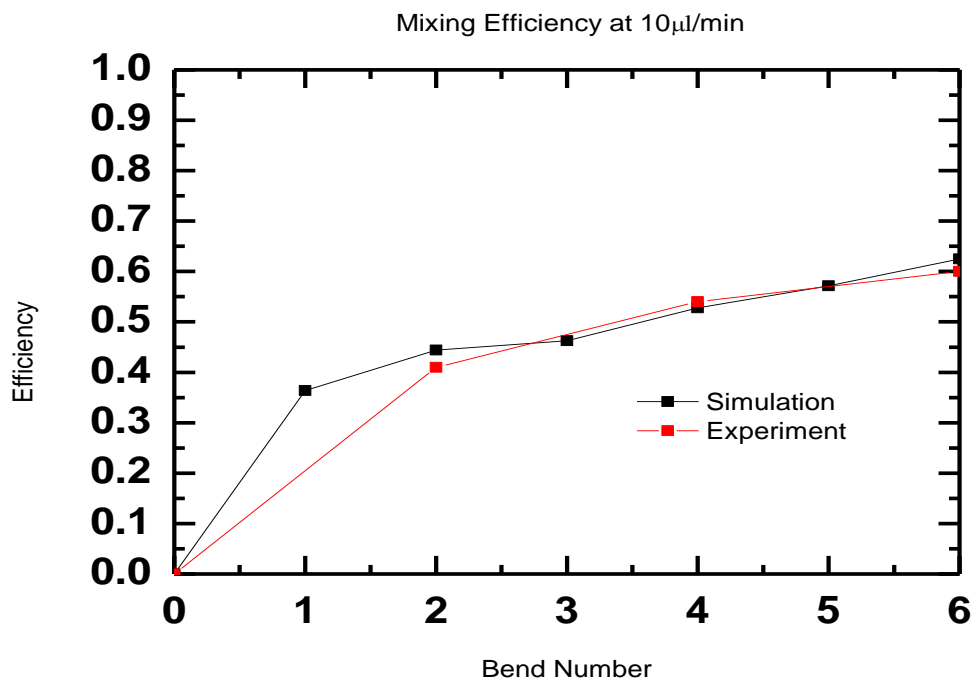


Figure 4.7 Mixing efficiency at Flow rate= $10\mu\text{l}/\text{min}$.

From the mixing efficiency plot, it is observable some mixing is happening regarding diffusion with an increase in bends, but complete mixing was not happening. Similar results are observed in simulation also. So the flow rate has been varied to find out the better mixing.

The experiment was again conducted at $0.1\mu\text{l}/\text{ml}$. The Figure 4.8a is the fluorescent image taken near inlet at the flow rate of $0.1\mu\text{l}/\text{ml}$, and the Figure 4.8b is the fluorescent image taken at the bend 2, and Figure 4.8c is taken at the bend 4, and Figure 4.8d is the fluorescent image at the bend 4. The bright region indicates the flow of dye mixed DI water and the dark region indicates the flow of the blank DI water. The channels have been highlighted with yellow dotted lines to know the boundary of channels. The Figures are observed as below.

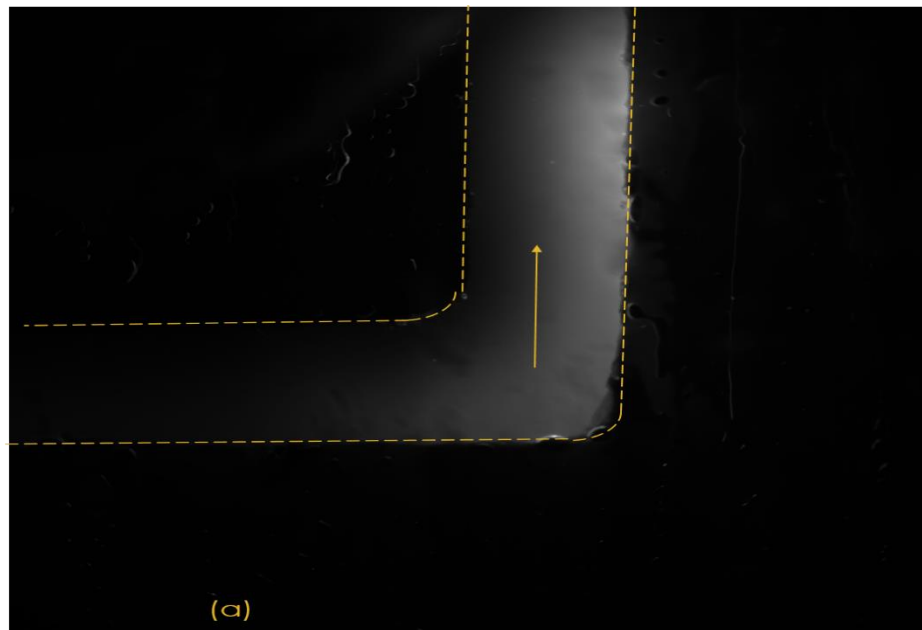


Figure 4.8a Fluorescent image near inlet at Flow rate= $0.1\mu\text{l}/\text{min}$.

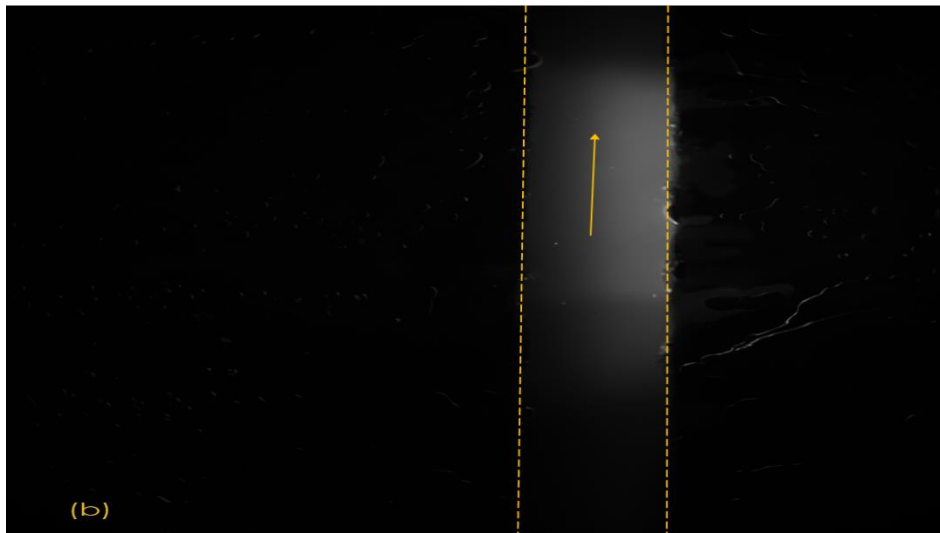


Figure 4.8b Fluorescent image at bend 2 at Flow rate= $0.1\mu\text{l}/\text{min}$.

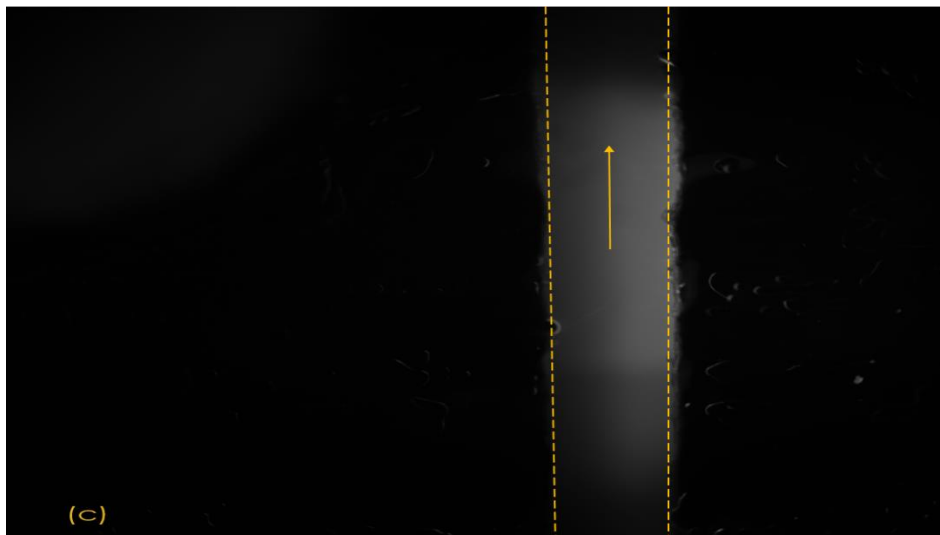


Figure 4.8c Fluorescent image at bend 4 at Flow rate= $0.1\mu\text{l}/\text{min}$.

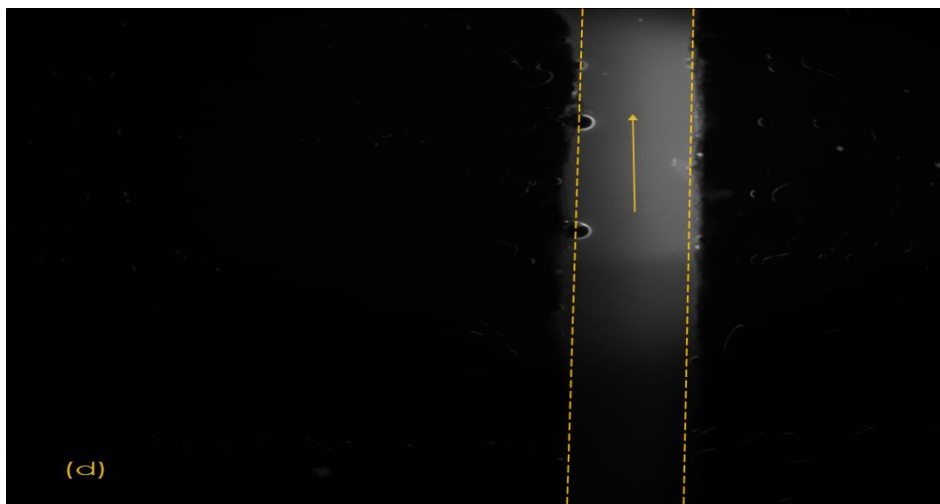


Figure 4.8d Fluorescent Image at Bend 6 at Flow rate= $0.1\mu\text{l}/\text{min}$.

From the above Figures its visible that the dye is getting diffused from one stream to another stream. In Figure 4.8a, both the streams started to diffuse, with the progress of bend, bright region in the image is significantly moving towards the left side from the right side as an indication of diffusion. The entire channel can be observed as a bright region which signifies mixing is happening.

The simulation for this flow is done at same parameters to verify the results which are done both in simulation and experiment are agreeing up.

Table 4.5 Parameters of Microchannel Dimension

PARAMETERS	Value
Width of the channel	700 μ m
Depth of the channel	25 μ m
Number of Loops	3
Flow Rate	0.1 μ l/min

Figure 4.9 is the concentration Profile obtained from the COMSOL simulation for flow rate at 0.1 μ l/min. The concentration profile is agreeing up with the experimental profile based on visual observation.

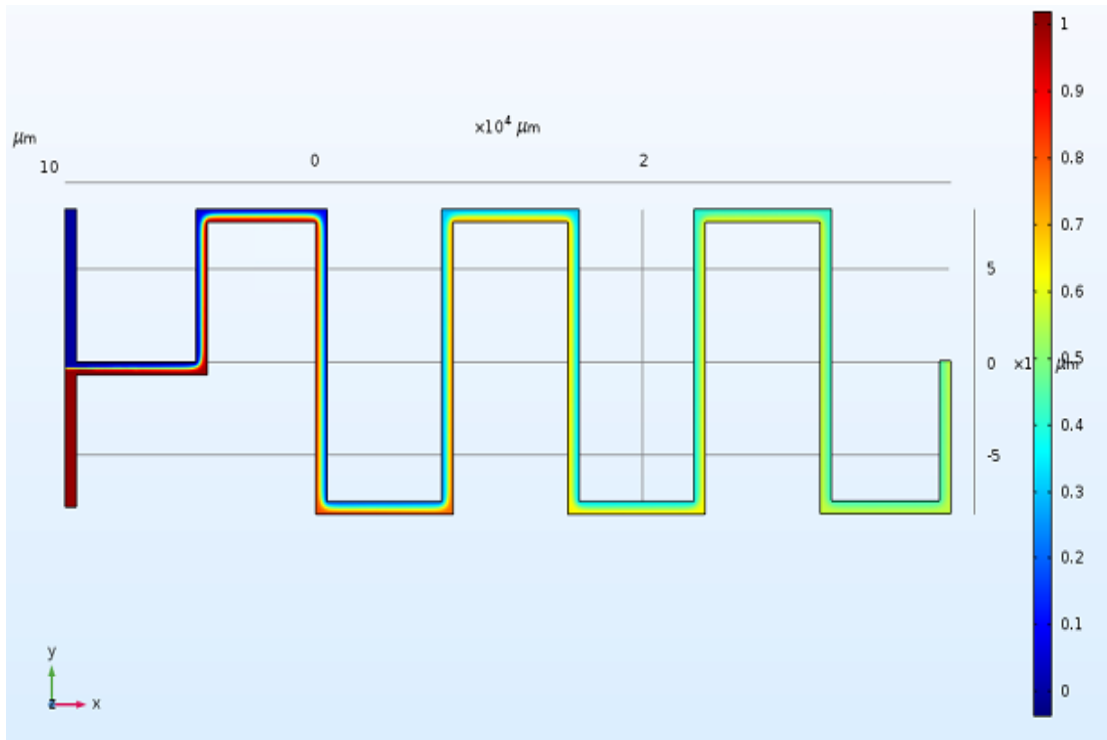


Figure 4.9 Predicted concentration Profile at Flow rate= 0.1 μ l/min.

In the COMSOL, results the red color indicates the molecules and the blue color indicates the blank region. As the bend progress, the red color is shifting to the blue color region significantly along the center and turns into green indicating the diffusion of molecules from one stream to other occurring.

The concentration values obtained along the bends are used to find the mixing efficiency at each bend at a flow rate of 0.1 μ l/min and have been plotted as a graph.

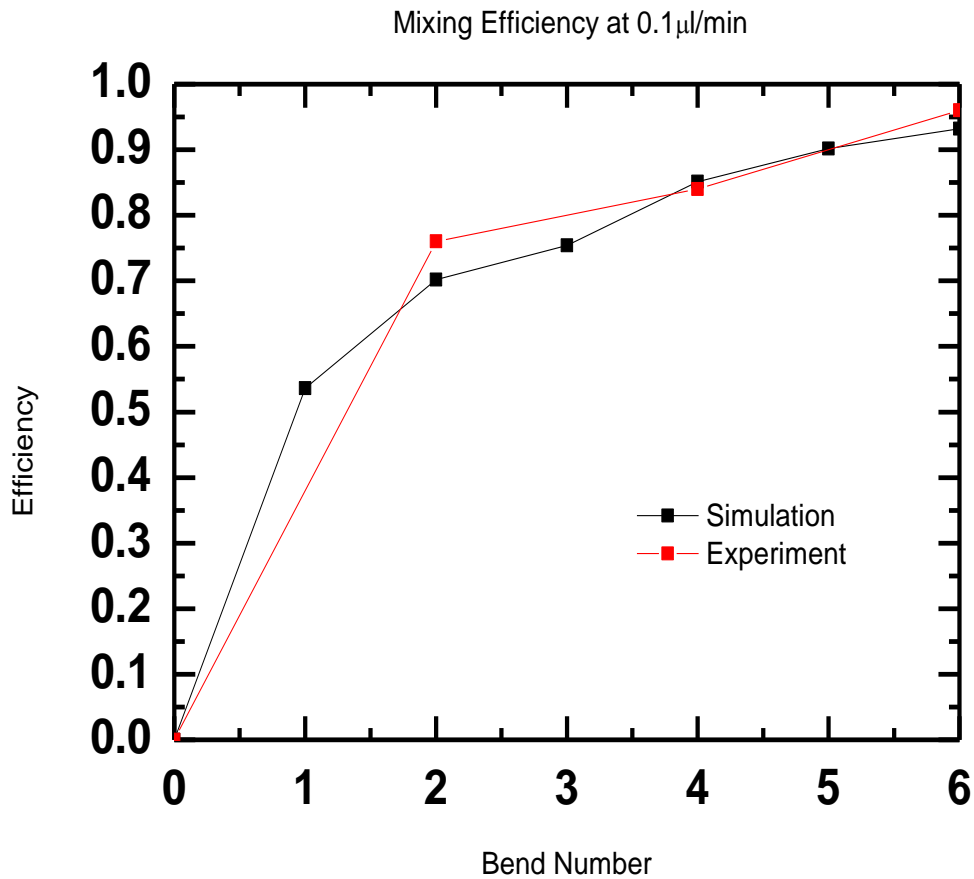


Figure 4.10 Mixing Efficiency at Flow rate=0.1 μ l/min.

The above results suggest that great increase in efficiency of mixing when the flow rate is decreased to 0.1 μ l/min.

The COMSOL simulation has been made by varying the depth of the channel to find better mixing at 10 μ l/min. The Reynolds number and the volume for the varying parameter have been tabulated in Table 4.5

Table 4.5 Values of Reynolds Number and Volume at Different Flow Rates

Depth (μ m)	Reynolds No. at 10 μ l/min	Reynolds No. 0.1 μ l/min	Volume (μ l)
25	0.05	5×10^{-4}	2.75
50	0.11	11×10^{-4}	5.51
100	0.2	20×10^{-4}	11.02
200	0.36	36×10^{-4}	22.05
400	0.59	59×10^{-4}	44.1

Table 4.6 Mixing Efficiency of Simulation at Flow Rate=10 μ l/min

Bend Number	Depth at 25 μ m	Depth at 50 μ m	Depth at 100 μ m	Depth at 200 μ m	Depth at 400 μ m
0	0	0	0	0	0
1	0.36359	0.38764	0.46431	0.51316	0.62176
2	0.44407	0.45557	0.54898	0.65057	0.74197
3	0.48286	0.51851	0.62969	0.75483	0.82531
4	0.52804	0.57029	0.69723	0.8396	0.87974
5	0.57181	0.61952	0.77215	0.89219	0.91974
6	0.62486	0.66363	0.81408	0.92784	0.95539

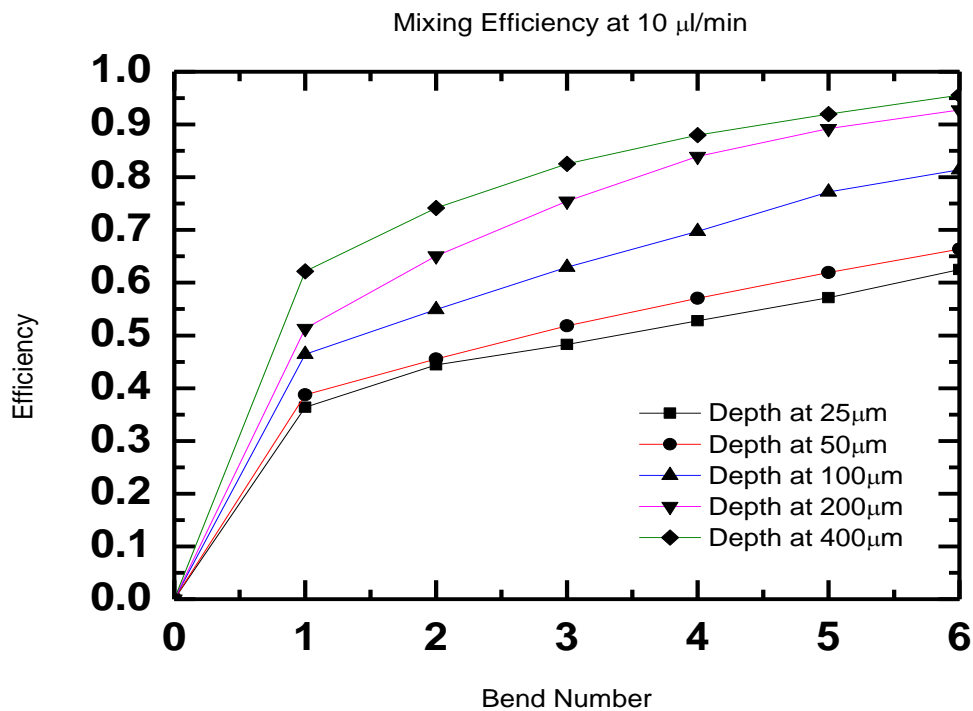


Figure 4.11 Mixing Efficiency of simulation at Flow rate= 10 μ l/min.

The Figure 4.11 is the graphical representation of the mixing at 10 μ l/min results obtained through COMSOL simulation.

The COMSOL simulation has been made by varying the depth of the channel to find better mixing at 10 μ l/min. The results have been tabulated in table 4.6.

Table 4.7 Mixing Efficiency of Simulation at Flow Rate=10 μ l/min

Bend Number	Depth at 25 μ m	Depth at 50 μ m	Depth at 100 μ m	Depth at 200 μ m	Depth at 400 μ m
0	0	0	0	0	0
1	0.53609	0.55631	0.61424	0.66786	0.75946
2	0.70188	0.69665	0.75345	0.82424	0.88262
3	0.78431	0.80585	0.85568	0.91438	0.94743
4	0.85143	0.86729	0.90926	0.95731	0.97431
5	0.90198	0.91493	0.95008	0.98002	0.98853
6	0.93188	0.94097	0.9685	0.99008	0.99548

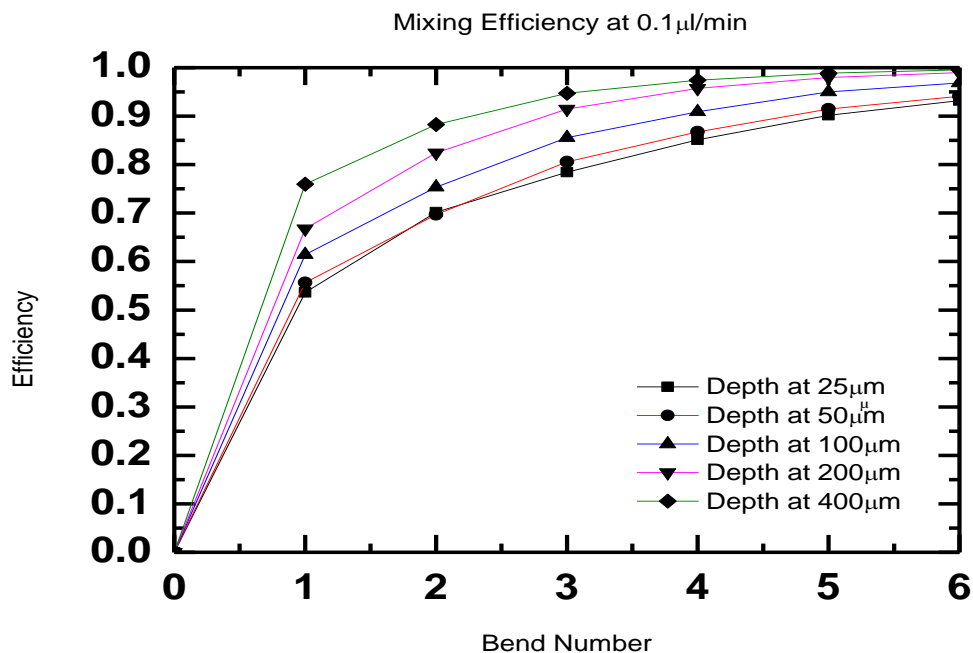


Figure 4.12 Mixing Efficiency of simulation at Flow rate=0.1 μ l/min.

The Figure 4.12 is the graphical representation of the mixing at 0.1 μ l/min results obtained through COMSOL simulation for varying depth (D).

CONCLUSION

There are lot of works done on the microfluidic passive mixing, though the use of cost effective adhesive tape for the design of mixing system make it valuable and novel. The experiment and simulation indicate that the mixing can be achieved regarding diffusion through the effective design of the channels. The parameters, which play an important role, are flow rate and depth of the channel, which helps in increasing the contact time between streams. As discussed in chapter 1, the contact time and flow rate indeed played an important role in diffusion. Therefore, by increasing the depth of the channel results in more contact area and increases diffusion, which resulted in better mixing. These shows passive mixing can also be made efficient with the use of Adhesive tape, which in turn will reduce the production, cost resulting from active mixing models.

The COMSOL simulation have been performed in the COMSOL Multiphysics 5.3. Using laminar flow and transport of diluted species physics with the same dimensions of microfluidic channel successfully using the governing equations and boundary equations.

Also, the simulation results from COMSOL have been compared with the experimental results and found to have a good correlation and the small deviation was observed due to the difference between ideality in simulation and experiment. Because of experimental correlation, the need for the real experiment has been reduced, and parameters can be optimized in the COMSOL itself.

CHAPTER 6

FUTURE WORK

The two inlet design of the microchannel can be used for analytical techniques in future since the mixing efficiency is achieved up to 96.5% in the design. The inlet channels can be injected with sample and fluorophore on each channel separately to perform sample analysis based on fluorescence if the selection of fluorophore and sample is based on the direct fluorescence, the results can be easily achieved in the microchannel. The work on direct fluorescence has already been done in microfluidic device [70]. The smaller dimensions of the microfluidic design can be used to perform high throughput analysis in diagnostics. In the need for high-velocity flow, the depth of the channel can be increased in a way where maximum efficiency can be achieved. So based upon the need, the parameters can be tweaked for the process. This method will be a novel approach since we are using adhesive tape for the fabrication of device and validated it for maximum efficiency. The microfluidic devices can also be used in the manufacturing of drugs such as Ibuprofen, which are suitable for continuous flow manufacturing. Ibuprofen was already been synthesized using PFA tubing's. The dimensions of the PFA tubing and the mixing efficiency in that system can be achieved in the microfluidic devices fabricated using adhesive tapes. It is also a viable future work aspect. The work can get spear headed in many direction due to the potential of application in many streams and because of its cost effectiveness.

APPENDIX A

COMSOL

To build the model in COMSOL Multiphysics using the governing equations, two physics interfaces are used: the Laminar Flow interface for laminar single-phase fluid flow and the Transport of Diluted species in Fluids interface. In this model, the equations are coupled in both directions. Pressure from Laminar.

MODELING INSTRUCTIONS:

Open COMSOL Multiphysics and click **Model Wizard**.

MODEL WIZARD:

1. In the **Model Wizard** window, click **3D**.
2. In the **Select physics** tree, select **Fluid flow>Single-Phase Flow>Laminar Flow (SPF)**.
3. Click **Add**.
4. Click **Study**.
5. In the **Select study** tree, select **Preset Studies for Selected Physics Interfaces>Stationary**.
6. In the **Select physics** tree, select **Transport of Diluted species**.
6. Click **Add**.
7. Click **Study**.
8. In the **Select study** tree, select **Preset Studies for Selected Physics Interfaces>Stationery**
9. Click **Done**.

DEFINITIONS:

Parameters

1. On the **Model** toolbar, click **Parameters**.

2. In the **Settings** window for Parameters, locate the **Parameters** section.
3. In the table, enter the following settings: H = 100um and L =500um (these parameters are used to do parametric sweeps).

GEOMETRY 1

1. Click geometry and in the settings window set the length unit to μm .

Part Library1 (blk 1)

1. On the **Geometry** toolbar, right click and choose **Part Library**.
2. Choose **Serpentine model 2D**
3. In the **Settings** window, locate the **Size** section.
4. Enter the value 700 and 25 respectively for the **width** and **depth**.
5. In the same **Settings** window, locate **Position** section and enter the following values:
X=0, Y=0.
5. Click the **Build All Objects** button.

Block 2 (blk 2)

1. On the **Geometry** toolbar, right click and choose **Rectangle**.
2. In the **Settings** window for Block, locate the **Size** section.
3. Enter the value 700 and 25 respectively for the **height** and **width**.
4. In the same **Settings** window, locate **Position** section and enter the following values:
X=29500, Y=0.
5. Click the **Build All Objects** button.

Block 3 (blk 3)

1. On the **Geometry** toolbar, right click and choose **Block**.
2. In the **Settings** window for Block, locate the **Size** section.
3. Enter the values 100, 30000 and 500 for the **height**, **width**, and **depth** respectively.
4. In the same **Settings** window, locate **Position** section and enter the following values:

X=0, Y=0, Z=0

5. Click the **Build All Objects** button.

ADD MATERIAL

1. On the **Model** toolbar, right click on **Materials** and select **Add Material** to open the **Add Material** window.

2. Go to the **Add Material** window.

3. In the tree, select **Built-In>Water, liquid**.

4. Click **Add to Component** in the window toolbar and close the **Add Material** window.

MULTIPHYSICS

1. On the **Physics** toolbar, click **Multiphysics** and choose **Global> Flow Coupling**.

LAMINAR FLOW (SPF)

No changes are done in the default tab **Fluid Properties 1**, **Initial values 1** and **Wall**

1. The default specifications in these tabs are true to the model in this study. Right-click on the **Laminar Flow** tab and select **Inlet** and **Outlet**.

Inlet 1

1. On the **Physics** toolbar, right click and choose **Inlet**

2. Select **Boundary 2** only.

3. In the **Settings** window for **Inlet**, locate the **Velocity** section.

1. The normal inflow velocity is chosen, and U_0 is given the values of 10^{-5} , 10^{-6} (used in this study)

Inlet 2

1. On the **Physics** toolbar, right click and choose **Inlet**

2. Select Boundary 5 only.
3. In the **Settings** window for **Inlet**, locate the **Velocity** section.
4. The normal inflow velocity is chosen, and U_0 is given the values of 10^{-5} , 10^{-6} (used in this study)

Outlet 1

1. On the **Physics** toolbar, right click and choose **Outlet**.
2. Select Boundary 24 only.
3. In the **Settings** window for **Outlet**, locate the Pressure Conditions section. The default pressure is 0 Pa and remains as such.
4. Select **Suppress backflow** check box.

Transport of Diluted species (Tds)

1. No changes are made in the default tabs, **Transport of Diluted species**.

Initial Values 1

1. In the **Model Builder** window, under **Component 1 (comp1)**> **Transport of Diluted species (tds)** click **Initial Values 1**
2. In the **Settings** window for Initial Values, locate the Initial Values section.
3. In the T text field, type 300K.

Concentration 1

1. On the **Physics** toolbar, right click and choose concentration
2. Select Boundary 2 only.
3. In the **Settings** window for **Concentration**, locate the **species** section.
4. Enter $c_0=1\text{mol/m}^3$

Concentration 2

1. On the **Physics** toolbar, right click and choose concentration
2. Select Boundary 5 only.
3. In the **Settings** window for **Concentration**, locate the **species** section.

4. Enter $c_0=0\text{mol/m}^3$

Outlet 1

1. On the **Physics** toolbar, right click and choose **Outlet**.
2. Select Boundary 24 only.
3. In the **Settings** window for **Outlet**, locate the Pressure Conditions section. The default pressure is 0 Pa and remains as such.
4. Select **Suppress backflow** check box.

MESH 1

1. In the **Model Builder** window, under **Component 1 (comp1)** click **Mesh 1** and select **User Controlled Mesh**

Size

1. In the **Settings** window, select **Fine Mesh**.

Size 1

1. In the **Settings** window, select **Finer Mesh** and select Boundary 14 only.
2. Click **Mesh 1** and click **Build All**.

STUDY 1

Since the study will automatically generate a large number of default plots, default plots are disabled.

1. In the Settings window for Study, locate the Study Settings section.
2. Clear the Generate default plots check box.

For Step 1, solve only the creeping flow problem.

Step 1: Stationary 1

1. In the Model Builder window, under Study 1 click Step 1: Stationary.
2. In the Settings window for Stationary, locate the Physics and Variables Selection section.
3. In the table, clear the Solve for checkbox for the Transport of Diluted Species interface. Add a second study step.

Step 2: Stationary

1. On the Study toolbar, click Study Steps and choose Stationary>Stationary. Disable the solution of the creeping flow problem for this step, but import the previously computed solution into the relevant dependent variables so that they can be used to compute the convective species transport.
2. In the Settings window for Stationary, locate the Physics and Variables Selection section.
3. In the table, clear the Solve for checkbox for the Creeping Flow interface. Click to expand the Values of dependent variables section. Locate the Values of Dependent Variables section. Find the Values of variables not solved for the subsection. From the Settings list, choose User controlled.
4. From the Method list, choose Solution. 6 From the Study list, choose Study 1, Stationary

RESULTS

1. After the Simulation is run, the default plots are generated namely; **Concentration**, **Velocity**, and **Pressure**. These nodes are present in the **Results** node.

Concentration values.

1. The **Results** are shown in a table under the **Graphics** window, which can be exported as a text file or read immediately.

REFERENCES

1. Lin B. *Microfluidics: technologies and applications*: Springer; 2011.
2. Wu J, Kodzius R, Cao W, Wen W. Extraction, amplification and detection of DNA in microfluidic chip-based assays. *Microchimica Acta*. 2014;181:1611-31.
3. Fan A, Byrnes S, Klapperich C. Purification of DNA/RNA in a microfluidic device. *Microfluidic Diagnostics: Methods and Protocols*. 2013:403-11.
4. Kakuta M, Bessoth FG, Manz A. Microfabricated devices for fluid mixing and their application for chemical synthesis. *The Chemical Record*. 2001;1:395-405.
5. Capretto L, Cheng W, Hill M, Zhang X. Micromixing within microfluidic devices. *Microfluidics*: Springer; 2011. p. 27-68.
6. Buchegger W, Wagner C, Lendl B, Kraft M, Vellekoop MJ. A highly uniform lamination micromixer with wedge shaped inlet channels for time resolved infrared spectroscopy. *Microfluidics and Nanofluidics*. 2011;10:889-97.
7. Koch M, Chatelain D, Evans A, Brunnschweiler A. Two simple micromixers based on silicon. *Journal of Micromechanics and Microengineering*. 1998;8:123.
8. Bessoth FG, Manz A. Microstructure for efficient continuous flow mixing. *Analytical communications*. 1999;36:213-5.
9. Kenis PJ, Ismagilov RF, Whitesides GM. Microfabrication inside capillaries using multiphase laminar flow patterning. *Science*. 1999;285:83-5.
10. Weigl BH, Bardell R, Schulte T, Battrell F, Hayenga J. Design and rapid prototyping of thin-film laminate-based microfluidic devices. *Biomedical Microdevices*. 2001;3:267-74.
11. Losey MW, Jackman RJ, Firebaugh SL, Schmidt MA, Jensen KF. Design and fabrication of microfluidic devices for multiphase mixing and reaction. *Journal of Microelectromechanical Systems*. 2002;11:709-17.
12. Lin CH, Tsai CH, Fu LM. A rapid three-dimensional vortex micromixer utilizing self-rotation effects under low Reynolds number conditions. *J. Micromech. Microeng.* 2005; 15:935–943.
13. Tofteberg T, Skolimowski M, Andreassen E, Geschke O. A novel passive micromixer: Lamination in a planar channel system. *Microfluid. Nanofluid.* 2010; 8:209–215.
14. Branbjerg J. From microfluidic components to micro-TAS. *Proceedings of Micro Total Analysis System Workshop*; Enschede, the Netherlands. 21–22 November 1994.
15. Scampavia LD, Blankenstein G, Ruzicka J, Christian GD. A coaxial jet mixer for rapid kinetic analysis for chemical and biological microreactors. *Anal. Chem.* 1995; 67:2743–2749

16. Wong SH, Ward MCL, Wharton CW. Micro T-mixer as rapid mixing micromixer. *Sens. Actuators B*. 2004; 100:359–379.
17. Mengeaud V, Josserand J, Girault HH. Mixing processes in a zigzag microchannel: Finite element simulations and optical study. *Anal. Chem*. 2002; 174:4279–4286.
18. Hong CC, Choi JW, Ahn CH. A novel in-plane passive microfluidic mixer with modified Tesla structures. *Lab Chip*. 2003; 4:109–113.
19. Vijayendran RA, Motsegood KM, Beebe DJ, Leckband DE. Evaluation of a three-dimensional micromixer in a surface-based biosensor. *Langmuir*. 2003; 19:1824–1828.
20. Chen Z, Bown MR, O’Sullivan B, MacInnes JM, Allen RWK, Mulder M, Blom M, van’t Oever R. Performance analysis of a folding flow micromixer. *Microfluid. Nanofluid.* 2009; 7:783–794.
21. Kang TG, Singh MK, Anderson PD, Meijer HEH. A Chaotic Serpentine Mixer Efficient in the Creeping Flow Regime: From Design Concept to Optimization. *Microfluid. Nanofluid.* 2009; 6:763–774.
22. Moon D, Migler KB. Forced assembly and mixing of melts via planar polymer micro mixing. *Polymer*. 2010; 51:3147–3155.
23. Liu YZ, Kim BJ, Sung HJ. Two-fluid mixing in a microchannel. *Int. J. Heat Fluid Flow*. 2004; 25:986–995.
24. Jen CP, Wu CY, Lin YC, Wu CY. Design and simulation of the micromixer with chaotic advection in microchannels. *Lab Chip*. 2003; 3:77–81.
25. Jen CP, Wu CY, Lin YC, Wu CY. Design and simulation of the micromixer with chaotic advection in microchannels. *Lab Chip*. 2003; 3:77–81.
26. Park SJ, Kim JK, Park J, Chung S, Chung C, Chang JK. Rapid three-dimensional passive rotation micromixer using the breakup process. *J. Micromech. Microeng.* 2004; 14:6–14.
27. Aubin J, Fletcher DF, Xuereb C. Design of micromixers using CFD modelling. *Chem. Eng. Sci.* 2005; 60:2503–2516.
28. Yang JT, Huang KJ, Lin YC. Geometric effects on fluid mixing in passive grooved micromixers. *Lab Chip*. 2005; 5:1140–1147.
29. Hardt S, Pennemann H, Schonfeld F. Theoretical and experimental characterization of a low-Reynolds number split-and-recombine mixer. *Microfluid. Nanofluid.* 2006; 2:237–248.
30. Chen Z, Bown MR, O’Sullivan B, MacInnes JM, Allen RWK, Mulder M, Blom M, van’t Oever R. Performance analysis of a folding flow micromixer. *Microfluid. Nanofluid.* 2009; 7:783–794.

31. Kang TG, Singh MK, Anderson PD, Meijer HEH. A Chaotic Serpentine Mixer Efficient in the Creeping Flow Regime: From Design Concept to Optimization. *Microfluid. Nanofluid.* 2009; 6:763–774.
32. Singh MK, Anderson PD, Meijer HEH. Understanding and optimizing the SMX static mixer. *Macromol. Rapid Commun.* 2009; 30:362–376.
33. Tsai R, Wu C. An efficient micromixer based on multidirectional vortices due to baffles and channel curvature. *Biomicrofluidics.* 2011; 5:014103.
34. Hardt S, Pennemann H, Schonfeld F. Theoretical and experimental characterization of a low-Reynolds number split-and-recombine mixer. *Microfluid. Nanofluid.* 2006; 02:237–248.
35. Mason BP, Price KE, Steinbacher JL, Bogdan AR, McQuade DT. Greener approaches to organic synthesis using microreactor technology. *Chemical reviews.* 2007; 107:2300-18.
36. Hessel V, Lob P, Lowe H. Development of microstructured reactors to enable organic synthesis rather than subduing chemistry. *Current Organic Chemistry.* 2005; 9:765-87.
37. Hessel V, Löwe H. Organic synthesis with microstructured reactors. *Chemical engineering & technology.* 2005; 28:267-84.
38. Hodge P. Organic synthesis using polymer-supported reagents, catalysts and scavengers in simple laboratory flow systems. *Current opinion in chemical biology.* 2003; 7:362-73.
39. Jas G, Kirschning A. Continuous flow techniques in organic synthesis. *Chemistry-A European Journal.* 2003; 9:5708-23.
40. Kirschning A, Altwicker C, Dräger G, Harders J, Hoffmann N, Hoffmann U, et al. PASSflow Syntheses Using Functionalized Monolithic Polymer/Glass Composites in Flow-Through Microreactors. *Angewandte Chemie International Edition.* 2001; 40:3995-8.
41. Pennemann H, Watts P, Haswell SJ, Hessel V, Löwe H. Benchmarking of microreactor applications. *Organic Process Research & Development.* 2004; 8:422-39.
42. Bogdan AR, Poe SL, Kubis DC, Broadwater SJ, McQuade DT. The Continuous-Flow Synthesis of Ibuprofen. *Angewandte Chemie International Edition.* 2009; 48:8547-50.
43. Watts P, Wiles C. Micro reactors: a new tool for the synthetic chemist. *Organic & biomolecular chemistry.* 2007; 5:727-32.
44. Fukuyama T, Rahman MT, Sato M, Ryu I. Adventures in inner space: Microflow systems for practical organic synthesis. *Synlett.* 2008; 2008:151-63.
45. Ahmed-Omer B, Brandt JC, Wirth T. Advanced organic synthesis using microreactor technology. *Organic & biomolecular chemistry.* 2007; 5:733-40.

46. Yu L, Pan Y, Wang C, Zhang L. A two-phase segmented microfluidic technique for one-step continuous versatile preparation of zeolites. *Chemical Engineering Journal*. 2013; 219:78-85.
47. Sultana M. Microfluidic systems for continuous crystallization of small organic molecules. *Microfluidic systems for continuous crystallization and in situ detection of small organic molecules* 2010.
48. Bonfils F, Cazaux I, Hodge P, Caze C. Michael reactions carried out using a bench-top flow system. *Organic & biomolecular chemistry*. 2006; 4:493-7.
49. Yoshida Ji, Nagaki A, Yamada T. Flash chemistry: fast chemical synthesis by using microreactors. *Chemistry-A European Journal*. 2008; 14:7450-9.
50. Nagaki A, Takabayashi N, Tomida Y, Yoshida J-i. Selective monolithiation of dibromobiaryls using microflow systems. *Organic letters*. 2008; 10:3937-40.
51. Yoshida Ji, Kim H, Nagaki A. Green and sustainable chemical synthesis using flow microreactors. *ChemSusChem*. 2011; 4:331-40.
52. Linden JJvd, Hilberink PW, Kronenburg CM, Kemperman GJ. Investigation of the Moffatt– Swern oxidation in a continuous flow microreactor system. *Organic Process Research & Development*. 2008;12:911-20.
53. Fox ER, Sweet BV, Jensen V. Drug shortages: a complex health care crisis. *Mayo Clinic Proceedings: Elsevier*; 2014. p. 361-73.
54. Hopkin MD, Baxendale IR, Ley SV. An expeditious synthesis of imatinib and analogues utilising flow chemistry methods. *Organic & biomolecular chemistry*. 2013; 11:1822-39.
55. Ende am DJ. Chemical engineering in the pharmaceutical industry: an introduction. *Chemical Engineering in the Pharmaceutical Industry: R&D to Manufacturing*. 2011:1-20.
56. Swenson G. President's Council of Advisors on Science and Technology. 2015.
57. McDaniel K, Roman G, Culbertson C. Development of novel coatings for PDMS-BASED microfluidic devices. *Abstracts of Papers of the American Chemical Society: AMER CHEMICAL SOC 1155 16TH ST, NW, WASHINGTON, DC 20036 USA*; 2005. p. U374-U5.
58. Chan CPY, Mak WC, Cheung KY, Sin KK, Yu CM, Rainer TH, et al. Evidence-based point-of-care diagnostics: current status and emerging technologies. *Annual review of analytical chemistry*. 2013;6: 191-211.
59. Kumar S, Kumar S, Ali M, Anand P, Agrawal VV, John R, et al. Microfluidic-integrated biosensors: Prospects for point-of-care diagnostics. *Biotechnology journal*. 2013; 8:1267-79.
60. Song P, Hu R, Tng DJH, Yong K-T. Moving towards individualized medicine with microfluidics technology. *Rsc Advances*. 2014; 4:11499-511.

61. John D, Anderson J. Computational fluid dynamics: the basics with applications. P Perback, International ed, Published. 1995.
62. Jännig O, Nguyen N-T. A polymeric high-throughput pressure-driven micromixer using a nanoporous membrane. *Microfluidics and nanofluidics*. 2011; 0:513-9.
63. Cha J, Kim J, Ryu S-K, Park J, Jeong Y, Park S, et al. A highly efficient 3D micromixer using soft PDMS bonding. *Journal of Micromechanics and Microengineering*. 2006; 16:1778.
64. Khan WA, Yovanovich MM. Analytical modeling of fluid flow and heat transfer in microchannel/nanochannel heat sinks. *Journal of Thermophysics and Heat Transfer*. 2008; 22:352-9.
65. Wadgaonkar, I., & Arikapudi, S. Modeling of Humidification in Comsol Multiphysics 4.4.
66. Negi, V. S. (2013). *NUMERICAL STUDY OF MICROSCALE HEAT SINKS USING DIFFERENT SHAPES & FLUIDS*. Paper presented at the COMSOL Bangalore, India.
67. Patsis G, Petropoulos A, Kaltsas G. Modelling and evaluation of a thermal microfluidic sensor fabricated on plastic substrate. *Microsystem technologies*. 2012; 18:359-64.
68. Liu D, Garimella SV. Analysis and optimization of the thermal performance of microchannel heat sinks. *International Journal of Numerical Methods for Heat & Fluid Flow*. 2005; 15:7-26.
69. Trethewey DC, Meinhart CD. Apparent fluid slip at hydrophobic microchannel walls. *Physics of fluids*. 2002; 14:L9-L12.
70. Tsukagoshi K, Hattori Y, Hayashi T, Nakajima R, Yamashita K, Maeda H. Micro-channel chemiluminescence analysis using a peroxyoxalate reaction that works through liquid-liquid interface collapse under laminar-flow conditions. *Analytical Sciences*. 2008; 24:1393-8.